

CONTENTS

1	INTRODUCTION	1
2	BIOLOGY	3
3	GRAPH THEORY	5
3.1	Directed graphs	5
3.2	Network measures	8
3.3	Random Graph Theory	9
3.4	Geometric Graphs	11
4	NETWORK MODEL	17
4.1	Overview	17
4.2	Anisotropy in Neural Connectivity	18
4.3	Anisotropic geometric network model	23
4.4	Numerical Implementation	25
4.5	Distance dependent connectivity	27
4.6	Rewiring	29
4.7	Anisotropy Measure	33
4.8	Summary and Discussion	34
5	STRUCTURAL ASPECTS	35
5.1	Introduction	35
5.2	Degree distribution	39
5.3	Small World Properties	42
5.4	Two Neuron Connections	43
5.5	Tuning distance-dependency	46
5.6	Motifs	49
I	APPENDIX	55
A	APPENIDX	57
A.1	Mathematica	57
A.2	Supplementary figures	58

LIST OF FIGURES

- Figure 3.1 **Typical examples of the directed graph types** **A)** directed pseudograph **B)** directed multi-graph **C)** directed loop graph **D)** simple directed graph. 6
- Figure 4.1 18
- Figure 4.2 **Tracing axonal branching of a pyramidal cell** In a 3-D model reconstructed from biocytin-labeled thick-tufted layer 5 pyramidal cells in the somatosensory cortex of postnatal (day 14) Wistar rats, Romand et al. (2011) depict dendritic compartments in red, axonal compartments in blue. **A)** A 600 μm window centered on the soma of the pyramidal cell shows the main stem of the cell's axon projecting downwards in a straight line, collaterals branching at various angles. **B)** Using image manipulation software, axon morphology was manually traced and is emphasized in black. 19
- Figure 4.3 **Illustrating axonal branch density** In a sample of 5 reconstructions from thick-tufted layer 5 pyramidal cells (Romand et al. 2011), tracing axonal morphology illustrates characteristic branch density along the axon's main stem. **A)** Example of extracted axonal tree. Outline manually traced using image manipulation software. Soma indicated by triangle. Original data from Romand et al. (2011). **B)** Overlaying 5 axonal trees extracted as in A), applying a Gaussian filter and displaying high axon densities in warm colors, illustrates the characteristic higher branch densities along the axon's main stem. 20

Figure 4.4

Dendritic morphology and branch density
 Using neuronal morphology of thick-tufted layer 5 pyramidal cells recorded by Romand et al. (2011), dendritic anatomy is traced and combined to illustrate high branch density around the soma. **A)** In a 600 μm window centered on the soma, basal dendrites (red) are visible extending around the soma. The ascending thick apical dendrite (red) is cut off and apical tuft is not shown. **B)-C)** Manual tracing of dendritic outlines in five samples (one shown), allows for clearer identification of stereotypical morphology and later analysis. **D)** Combining 5 dendritic outlines as shown in C) and subsequent Gaussian filtering reveals the relatively high dendritic branch density around the soma. 21

Figure 4.5

Connected neurons of a single pyramidal cell align with axonal projection Reducing the full axonal (blue, cf. Figure 4.2) and dendritic trees (red, gray, cf. Figure 4.4) as shown for two neurons in A) to their stereotypical axonal (blue) and dendritic profiles (red, gray) in B), demonstrates how connected neurons (red) tend to cluster around the pre-synaptic axon's profile, as spatial closeness constitutes a necessary condition for the formation of contacts. Unconnected neurons (gray) are found distant from the axon's projection, but not necessarily distant from the soma. 22

Figure 4.6

Anisotropic geometric network model and interpretations of width parameter w Illustrating the process of finding connections for one neuron (large triangle, black), the axon describes a linear trajectory in an arbitrary direction and until terminating on the surface's edge. Target neurons (red) are encountered along the path within a (here constant) distance w , which is in **A)** interpreted as a dendritic radius or, equivalently, in **B)** as a “bandwidth” of the axon. Connections to the encountered targets are then established as projections in **C)**, consistent with the directed nature of synapses in biological networks (cf. Chapter 2). 23

Figure 4.7

Axon width dependent connection probability determines parameter for numerical analysis Generating anisotropic networks with different axon widths w and extracting probability p of directed connection between two random nodes, demonstrates the dependency of p on the width parameter w . **A)** At an axon width of over $w = 100$, exceeding the square's side length, the connection probability saturates at $p = 0.5$, as axon bands are essentially “cutting” the square in a connected and unconnected half (c5b64f3e). **B)** For small w the connection probability is a linear function of w , allowing the width $w_S/2$ at which $p(w_S) = 11.6$ to be determined by a linear fit as $w_S/2 = 12.6$ (585a946f). [26](#)

Figure 4.8

Illustrating the proof of Theorem 4.3 Distance-dependent connectivity profile $C(x)$ in an anisotropic geometric graph calculated from geometric dependencies. **A)** In the case of $x \leq w/2$, target v' may be located anywhere on the shown semi-circle and therefore receives input from v with probability $1/2$. **B)** For $x > w/2$, suitable positions for target v' are dependent on x . The geometric relation $\sin \theta = w/2x$ leads to the distance-dependent connectivity profile as described in Theorem 4.3. [28](#)

Figure 4.9

Predicted distance-dependent connection probability profile is matched by numerical results Averaging distance-dependent connection probabilities over the 25 sample graphs, we find the expected profile calculated in Theorem 4.3 is matched perfectly by the numerical results. (dbffa88e) [29](#)

Figure 4.10

Rewiring transforms anisotropic geometric graphs to networks with isotropic connectivity For a given edge e with a distance x from its source vertex v to its target vertex $t(e)$, potential new targets (striped) are found in within a distance $(x - \varepsilon, x + \varepsilon)$ of v . The rewired edge then projects from v to a new target $t'(e)$, randomly chosen from the set of vertices within in this range. Inter-vertex distance between v and $t'(e)$ differs by less than ε from x , ensuring that for small ε the original distance-dependent connectivity is preserved. (Note that all targets within range are eligible for rewiring as no other edges exist. In general this is not the case.) 30

Figure 4.11

Rewiring with $\varepsilon = 1.25$ preserves distance-dependent profile in sample graphs Comparing the distance-dependent connection probabilities of the original graph (Theorem 4.3) in red with extracted of probabilities from the rewired ($\varepsilon = 1.25$) sample graphs in gray (errorbars SEM) we verify that distance-dependent connectivity is preserved when rewiring. The green curve shows the expected difference between the original and rewired distance profiles as estimated in Equation 4.1. (4f4dfcf1) 32

Figure 4.12

illustrate varying levels of anisotropy 33

Figure 4.13

Rewiring significantly reduces anisotropy In data taken from the 25 sample graphs (Section 4.4), vertex isotropy degree distribution is shown for the original set of graphs ($\eta = 0$). The characteristic highly anisotropic profile found in the original is already significantly reduced by partial rewiring; anisotropy degree distribution in the fully rewired graphs resemble degree distribution of equivalent purely distance-dependent networks. 33

Figure 5.1 Song et al. use quadruple whole-cell recordings, observing simultaneously the membrane potential of four neurons. **A)** Contrast image showing four thick-tufted L5 neurons **B)** Fluorescent image of the same cells after patching on **C)** Evoking an action potential in the presynaptic neuron causes characteristic membrane potential change in the postsynaptic neuron **D)** Inferring synaptic connectivity from the EPSP waveform observed in C). Image from (Song et al. 2005). 36

Figure 5.2 **In-degree distribution in anisotropic networks shows comparably high variance and is skewed to the left** From 250 anisotropic networks in-degree distributions were extracted and are shown in a normed histogram plot, errorbars SEM. Comparison with the binomial degree distribution (red) of a Gilbert random graph model with matching parameter set ($N = 1000$, $p = 0.116$) shows higher variance of in-degrees in anisotropic networks (sample variance = 344.54, variance of binomial distribution $Np(1 - p) = 102.44$.) Skewness to the left of the sample is -0.1763 . (9326138e) 39

Figure 5.3 **In-degree distribution not affected by varying degrees of anisotropy** In-degree distributions from the 25 sample graphs and their rewiring stages are plotted in normed histograms and listed from rewiring factor $\eta = 0$ (original anisotropic) to $\eta = 1$ (completely rewired, maximal isotropy). Comparison shows that varying degrees of anisotropy do not influence the degree distribution, in fact in-degree distributions match with the degree distribution of an equivalent distance-dependent network shown bottom-right (77995b6b). 40

- Figure 5.4 **Out-degree distribution not affected by varying anisotropy but highly different from distance-dependent networks** Out-degree distributions from the 25 sample graphs and their rewiring stages are plotted in normed histograms and listed from rewiring factor $\eta = 0$ (original anisotropic) to $\eta = 1$ (completely rewired, maximal isotropy). While varying degrees of anisotropy do not influence the degree distribution, the characteristic out-degree profile is drastically different from the distribution found in equivalent distance-dependent networks (77995b6b). 41
- Figure 5.5 **Characteristic out-degree distribution as an artifact of network's boundaries** From 250 anisotropic networks out-degree distributions were extracted and are shown in a normed histogram plot, errorbars SEM. The characteristic distribution is identified as an artifact of the network's spatial confinement; using equation 5.1 the out-degree profile is approximated (red) by the distribution of axon lengths in the anisotropic network (019555b0). 41
- Figure 5.6 **Anisotropy does not contribute to small-worldness** In increasingly rewired networks, trends show a decreasing average path length and rising clustering coefficient and thus possibly a higher degree of small-worldness in the rewired, isotropically connected networks. **A)** Average path lengths for network sizes $N = 250, 500$ and 1000 , where vertex pairs with no existing are discarded. Individual value pairs are obtained by averaging over a trial size of 20, 15 and 5 respectively; errorbars are SEM. **B)** Network configuration as in A), additionally showing clustering coefficients for distance-dependent networks. (064f9b10) 43

Figure 5.7

Overrepresentation of reciprocal connections in anisotropic networks due to distance-dependent connectivity Extracting the counts of unconnected, one-directionally and bidirectionally connected neuron pairs in the anisotropic sample graphs, overrepresentation of reciprocally connected pairs is identified as a feature of the network's distance dependency as opposed to anisotropy in connectivity. **A)** Showing the quotient of the counts for the three pair types, extracted from the set of sample graphs, with the number of expected pairs in Gilbert random graphs $G(n, p)$, where $n = 1000$ and $p = 0.116$ were matched to the sample graph parameters. While single connections appear less often than in Gilbert random graphs, reciprocal connections are significantly overrepresented. Errorbars SEM. **B)** Comparing appearance of connection pairs in the anisotropic sample graphs with their respective appearance in the rewired sample graphs, we find that eliminating anisotropy does not significantly change the counts for the connection types, indicating that anisotropy does not influence two neuron connection probabilities. Errorbars SEM. (c5f1462b) 45

Figure 5.8

Computing connection probability $C(x)$ from non-constant $w(x)$ 46

Figure 5.9

Network side length adjusted to match overall connection probability Side length of the network's surface determines the overall connection probability in the network when axon width function $w(x)$ is fixed. **A)** Connection probability declines with rising side length **B)** Determining side length as $s = 296 \mu\text{m}$ to match $p = 0.116$ as reported by Song et al. (2005). (6154302f, ef0e785d) 47

Figure 5.10

Anisotropic network model with tuned axon width $w(x)$ **A)** Resulting axon width function $w(x)$ from tuning to distance-dependent connection profile as reported by Perin et al. (2011), see also Figure 5.11. Note that $x \gg w(x)$ for most x , supporting approximation 5.4. **B)** Showing for a single neuron (star) connected (red) and unconnected (gray) neurons in the tuned anisotropic network, revealing the characteristic axon shape. (d45c02e4, 8f0d65e4) 48

Figure 5.11

Distance-independent overrepresentation of reciprocal connections Comparison of occurrences of one- and bidirectionally connected neuron pairs in the tuned anisotropic networks (gray) with profiles found by Perin et al. (red), shows that overrepresentation of bidirectional pairs is distance-independent and not connected to anisotropy. **A)** Overall connection probability in the tuned anisotropic networks was successfully adjusted to reflect connection probability found by Perin et al. **B)-C)** Showing in blue the probabilities to obtain a neuron pair motif (single edge in B, two edges in C) calculated under independence assumption from the overall probability from A), we find that counts in the tuned anisotropic networks (gray) match the independence assumption and do *not* show the overrepresentation present in Perin et al.'s experiment. (875505b0) 49

Figure 5.12

Relative occurrence of three-neuron patterns Extracting the counts of three-node motifs in anisotropic (filled bars) and distance-dependent networks (unfilled bars), the quotient of the obtained count with the number of occurrences expected from the two-neuron connection probabilities in the networks (cf. Section 5.4) shows the over- and underrepresentation of specific motifs in the network (red and black errorbars are SEM). In anisotropic networks pattern 12, for example, appears around five times more often than we would expect from the occurrence two-neuron connections. The relative counts for anisotropic networks resemble the findings of Song et al. (2005) and differ significantly from the counts in distance-dependent networks, implying that anisotropy has a strong influence on the relative occurrence of three-neuron patterns. (4839ce41) 51

Figure 5.13	Three-neuron motif occurrence in different network types	A) Comparing counts in anisotropic sample graphs with their rewired counterparts.
	B) Three-neuron motifs occurrence in tuned anisotropic networks (cf. Section 5.5) with their rewired counterparts. For this two-neuron connection probabilities were extracted as in Section 5.4 and motif probabilities were calculated analogously to anisotropic networks.	
	C) Relative counts for the high edge count motifs 15 and 16 for different network types, errorbars SEM.	
(4839ce41)	52	
(4afc2727)	58	
(c7ee86d7)	59	
Figure A.1	Average path length for anisotropic and distance-dependent networks, $N = 1000$.	
(064f9b10)	59	
Figure A.2	Probabilities for connections in neuron pairs are identical in distance-dependent and rewired anisotropic networks.	
(c5f1462b)	59	
Figure A.3		
Figure A.4		

LIST OF TABLES

LISTINGS

ACRONYMS

1

INTRODUCTION

2

BIOLOGY

3

GRAPH THEORY

A review of graph theory lays the foundation for the mathematical considerations in this work. Following the discussion of directed graphs as a basis for the networks introduced in this work, common network measures are reviewed. Random graph models are integral to this work and are discussed in Sections 3.3 and 3.4, the latter introducing geometric random graphs and performing geometric, probabilistic computations essential for the analytical discussions in later chapters.

3.1 DIRECTED GRAPHS

Here we introduce the various categories of directed graphs. The main reference for this section is [Bang-Jensen and Gutin \(2008\)](#), for the formal definition below however, we follow [nLab \(2014\)](#).

Definition 3.1 (Directed graphs). A *directed pseudograph* G consists of two finite V , the *set of vertices* of G , and E , the *set of edges* of G , and two maps $s, t : E \rightarrow V$, the *source* and *target functions* of G . A *directed multigraph* is a directed pseudograph without loops, that is the map $d = (s, t) : E \rightarrow V^2$ already maps to $V^2 \setminus \Delta_V$, where $V^2 = V \times V$ denotes the cartesian product and $\Delta_V = \{(x, x) \mid x \in V\} \subseteq V^2$ the diagonal. Similarly, a *directed loop graph* is a directed pseudograph where d is injective. Finally, a *simple directed graph* can be defined as a directed pseudograph where d is both injective and already maps to $V^2 \setminus \Delta_V$.

Thus, in simple directed graphs, neither parallel edges nor loops (edges between the same vertex) are allowed, whereas directed multigraphs and directed loop graphs admit one of them respectively. We refer to any of the four graph types simply as a directed graph and only specify the type when needed.

Given a directed graph G , we denote with $V(G)$ the set of vertices of G and call it the **vertex set** of G . Analogously, the **edge set** $E(G)$ of G denotes the set of edges of G . This means, for a directed graph specified as $G = (V, E, s, t)$, we have $V(G) = V$ and $E(G) = E$.

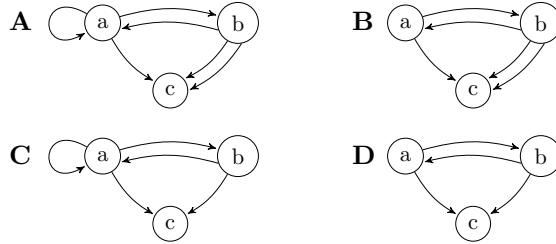


Figure 3.1: Typical examples of the directed graph types **A**) directed pseudograph **B**) directed multigraph **C**) directed loop graph **D**) simple directed graph.

A **morphism** $\phi : G \rightarrow H$, between two directed graphs $G = (V_G, E_G, s_G, t_G)$ and $H = (V_H, E_H, s_H, t_H)$, consists of a pair of maps $\phi_V : V_G \rightarrow V_H$ and $\phi_E : E_G \rightarrow E_H$, such that

$$s_H \circ \phi_E = \phi_V \circ s_G \quad \text{and} \quad t_H \circ \phi_E = \phi_V \circ t_G,$$

that is such that the following diagram commutes:

$$\begin{array}{ccc} E_G & \xrightarrow{\phi_E} & E_H \\ s_G \downarrow t_G & & \downarrow s_H t_H \\ V_G & \xrightarrow{\phi_V} & V_H \end{array}$$

A morphism $\varphi : G \rightarrow H$, between two directed pseudographs G and H is an **isomorphism**, if the maps $\varphi_V : V_G \rightarrow V_H$ and $\varphi_E : E_G \rightarrow E_H$ are bijections. Two directed pseudographs are called *isomorphic* if there exists an isomorphism inbetween them.

Remark. The last definition implies that, if there exists an isomorphism $\varphi : G \rightarrow H$, an isomorphism $\psi : H \rightarrow G$ can be found. This isomorphism is, of course, easily constructed via $\psi_V : V_H \rightarrow V_G, v \mapsto \varphi_V^{-1}(v)$, $\psi_E : E_H \rightarrow E_G, e \mapsto \varphi_E^{-1}(e)$.

Definition 3.2 (Weighted directed graphs). An *edge-weighted directed graph* is a directed graph G along with a mapping $\omega : E(G) \rightarrow \mathbb{R}$, called the *weight function*. Similarly, a *vertex-weighted directed graph* is a directed graph with a mapping $\nu : V(G) \rightarrow \mathbb{R}$.

Equivalent definiton for directed loop graphs

Remark. A directed graph G can be equivalently defined as a pair of finite sets V , the *set of vertices* of G , and $E \subseteq V^2$ the *set of edges* of G . For an edge $(x, y) \in E$, we call x the *source* and y the target of the edge (x, y) . Source and target functions are then uniquely determined as the projections on the first and second component,

$$s = \text{pr}_1, t = \text{pr}_2 : E(G) \rightarrow V.$$

Conversely, the edge set $E(G) \subseteq V^2$ can be determined from the source and target functions as $E := \{(s(e), t(e)) \mid e \in E\}$. The trivial identities $(x, y) = (\text{pr}_1(x, y), \text{pr}_2(x, y))$ and $\text{pr}_1(s(e), t(e)) = s(e)$ with

$\text{pr}_2(s(e), t(e)) = t(e)$ quickly verify the equivalence of the definitions. Given a directed loop graph G , we often assume the graph to be given in this form and write edges as $e = (x, y)$. Note that this concept is more complicated to introduce for directed pseudographs, since parallel edges e and Xe' should to be differentiated in the egde set of G , establishing the need for $E(G)$ to be a multi- or indexed set, notions we are trying to avoid in this document.

From now on any directed graph is assumed to be a directed loop graph. Although most, if not all, concepts work for directed pseudographs just as well, we want to start to heavily use the canonical edge representation, which when talking about pseudographs makes problems as mentioned before.

For a pair of vertex sets $X, Y \subseteq V(G)$ of a directed graph G we write

$$(X, Y)_G = \{(x, y) \in E(G) | x \in X, y \in Y\}$$

for the set of edges with source in X and target in Y . Specifically we write $T(x) = (x, V(G))_G$ for the set of *targets* for edges originating from the vertex x and $S(x) := (V(G), x)_G$ for the set of *sources* for edges projecting to x .

Notation for target and source sets

Definition 3.3 (In- and out-degree). For a directed graph G the **in-degree** $d_G^-(x)$ of a vertex x is defined as the number of edges of G with target x , that is

$$d_G^-(x) = |S(x)|.$$

Similarly, the **out-degree** $d_G^+(x)$ of x is defined as

$$d_G^+(x) = |T(x)|,$$

the number of edges in G with source x .

A basic property of the in- and out-degree in directed graphs is that number of in-degrees of every vertex, as well the sum of every out-degree, equal the total number of edges:

Proposition 3.4. *In every directed graph G , we have*

$$\sum_{x \in V(G)} d^-(x) = \sum_{x \in V(G)} d^+(x) = |E(G)|.$$

Proof. Since $(V(G), x)_G \cap (V(G), y)_G = \emptyset$ for $x \neq y$, we can write

$$\sum_{x \in V(G)} d^-(x) = \left| \bigcup_{x \in V(G)} (V(G), x)_G \right| = |(V(G), V(G))_G| = |E(G)|.$$

Analogously for the out-degree. \square

3.2 NETWORK MEASURES

Let G be a (simple) directed graph. A **walk** W in G is an alternating sequence $(x_1, e_1, x_2, e_2, x_3, \dots, x_{n-1}, e_{n-1}, x_n)$ of vertices x_i and edges e_i from G , such that

$$s(e_i) = x_i \quad \text{and} \quad t(e_i) = x_{i+1}, \quad \text{for } i = 1, \dots, n-1,$$

that is, such that the vertices are connected by the edges in between them. We denote the set of vertices (x_1, \dots, x_n) of W as $V(W)$ and the sequence of edges (e_1, \dots, e_{n-1}) as $E(W)$.

The vertices x_1 and x_n are called the *end vertices* of W and we also say that W is an (x, y) -walk. The **length** of W is defined as the length of the sequence of edges; a walk consisting of only one vertex has length zero.

Definition 3.5 (Distance). The **distance** of two vertices x, y in a directed graph G , is defined as the minimum length of an (x, y) -walk, if any such walk exists, otherwise $\text{dist}(x, y) = \infty$. In short,

$$\text{dist}(x, y) = \inf\{|E(W)| \mid W \text{ is } (x, y)\text{-walk}\}.$$

Proposition 3.6. *The distance function $\text{dist} : V(G) \times V(G) \rightarrow \mathbb{N}$ of a directed graph G satisfies the triangle equality,*

$$\text{dist}(x, z) \leq \text{dist}(x, y) + \text{dist}(y, z), \quad \text{for } x, y, z \in V(G).$$

Proof. Let x, y, z be vertices in G . If either no (x, y) -walk or (y, z) -walk exists, the inequality holds by definition. Otherwise, let W be an (x, y) -walk of minimal length and let U be a (y, z) -walk of minimal length. Certainly, by concatenating W and U we obtain an (x, z) -walk of length $|E(W)| + |E(U)| = \text{dist}(x, y) + \text{dist}(y, z)$, proofing that

$$\text{dist}(x, z) \leq \text{dist}(x, y) + \text{dist}(y, z).$$

□

Definition 3.7 (Average path length). The *average path length* of a directed graph G with $V(G) = n$ is defined as

$$l = \frac{1}{n(n-1)} \sum_{x \neq y \in V(G)} \text{dist}(x, y).$$

In practice, vertex pairs with $\text{dist}(x, y) = \infty$, that is pairs that are not connected by a walk, are disregarded in the computation and the average path length is determined in the connected components of the graph, ensuring that l is finite.

The concept of a small-world property in graphs was introduced by [Watts and Strogatz \(1998\)](#). Networks associated with the property are characterized by a small average path length, while however most nodes are organized in “cliques”, connecting to nodes that are themselves neighbors. A measure capturing this property is the (local) clustering coefficient:

Definition 3.8 (Clustering coefficient). The *clustering coefficient* of a vertex x in a directed graph G is defined as ratio of realized and possible edges between the neighbors of x . If N_x is the neighborhood of all vertices reciprocally connected to x ,

$$N_x = \{v \mid v \in T(x) \wedge v \in S(x)\},$$

then the clustering coefficient is given by

$$\text{clust}(x) = \frac{|(N_x, N_x)_G|}{|N_x|(|N_x| - 1)}.$$

Small-worldness is then described by a low average path length and high clustering coefficient, usually considered as the mean of all vertices.

3.3 RANDOM GRAPH THEORY

From this chapter on, as it is common and practical when talking about random graph models, we move away from the abstract notion of graphs and their equivalence classes and consider *labeled graphs*, where the edge set of a graph with n vertices takes the form $V = \{1, \dots, n\}$. Simple directed graphs constitute the fundamental mathematical object underlying the concepts developed in this work and if not specified otherwise, all graphs are assumed to be labeled and simple directed.

*focus on labeled,
simple directed
graphs*

The concept of a random graph was first formally introduced by [Erdős and Rényi \(1959\)](#). In their $G(n, N)$ model, a graph with n vertices and N edges is randomly and with equal probability selected from the set of such possible graphs. In the same year [Gilbert \(1959\)](#) independently introduced his $G(n, p)$ model, realizing edges between vertex pairs with a fixed probability p . The two models are closely related ([Luczak 1990](#)) and overlap in literature, both at times being referred to as *Erdős-Rényi graphs*. Here we focus on the $G(n, p)$ model, as it closer in concept to a computational implementation of a random graph. Defining it in detail in 3.9, we will refer to the random graph model as the *Gilbert random graph model*.

In general, a random graph model is a probability space over a set of graphs ([Janson et al. 2000](#)). Rather than specifying the sample space

and probability measure explicitly, random graph models are often defined by a random process that generates such graphs, leaving probability measure and sample space implicit (Bollobás 2001). The term *random graph*, in the graph theoretical context, refers to the random graph model itself. Especially in the computational context however, a random graph often refers to a single graph generated by a random process. Here we try to avoid this ambiguity and strictly refer to the mathematical object as a random graph model.

Keeping in mind that the term *graph* now refers to labeled, simple directed graphs if not otherwise specified we define G^n to be the set of simple directed graphs with n vertices,

$$G^n := \{G \mid G \text{ graph}, |V(G)| = n\}.$$

We first introduce Gilbert's random graph model $G(n, p)$ by explicitly defining a probability space over G^n and show later how the model may be realized as a random process.

Definition 3.9 (Gilbert random graph model). Let $n \in \mathbb{N}$ and $0 \leq p \leq 1$. The *Gilbert random graph model* $G(n, p)$ is a discrete probability space over G^n with event space $\mathcal{P}(G^n)$ and probability measure P , such that every graph G with $|E(G)| = k$ edges appears with equal probability

$$P(G) = p^k(1-p)^{n(n-1)-k},$$

for $0 \leq k \leq n(n-1)$.

Remark. Clearly $G(n, p)$ is well-defined, as there exist $\binom{n(n-1)}{k}$ distinct labeled graphs with n vertices and k edges and thus

$$\sum_{G \in G^n} P(G) = \sum_{k=0}^{n(n-1)} \binom{n(n-1)}{k} p^k (1-p)^{n(n-1)-k} = 1,$$

after the binomial theorem.

equivalent
definition as
random process

Equivalently, the Gilbert random graph model can be defined as a stochastic process; to an empty graph with n vertices, for each of the $n(n-1)$ vertex pairs an edge is added at random and independently with probability p . The probability to obtain a specific graph G with k edges is then obviously $p^k(1-p)^{n(n-1)-k}$, already proofing the equivalence, since assuming a process as above with edge probability p' such that the induced probability measure on G^n equals P from 3.9, already yields $p = p'$ in the choice of $n = 2$ and $k = 1$.

Proposition 3.10. *In- and out-degree distribution of vertices in the Gilbert random graph model are binomial.*

Proof. Let X be a random variable on the random graph model, mapping to the in-degree (out-degree) $d_G(v)$ of a vertex v of a graph $G \in G^n$. There are $n - 1$ other vertices that, with probability p , project to v (receive input from v), thus

$$P(X = k) = \binom{n-1}{k} p^k (1-p)^{n-1-k},$$

showing that $P^X = \mathcal{B}_{n-1,p}$. \square

The Gilbert random graph model is therefore also often referred to as *binomial random graph*. As typical neuronal networks are large ($n \geq 10^3$) with sparse connectivity ($p \approx 0.1$), in- and out-degree distribution can be approximated by a Poisson distribution, $P^X(k) \approx \text{Pois}_\lambda(k)$, with $\lambda = (n-1)p$, after the Poisson limit theorem.

Most results in the study of random graph models consider $n \rightarrow \infty$. In this study we are mostly interested in patterns of connectivity that arise in local circuits, leaving behind limit considerations and employ the Gilbert random graph model as a reference for the development of more detailed and specific random graph models.

3.4 GEOMETRIC GRAPHS

The theory of geometric graphs address the embedding of graphs in \mathbb{R}^d . Planar graphs are graphs that can be drawn on a surface with their edges drawn as straight lines between the vertices, such that no two lines intersect (Diestel 2000). Here we are interested in graphs embedded on surface. In the models introduced, connectivity then depends on geometric properties, such as distance between nodes or relative orientation between vertices. The basic graph type to allow for such connectivity rules is a geometric graph.

Definition 3.11 (Geometric directed graph). A *geometric directed graph* G_Φ is a directed graph G paired with a map

$$\Phi : V(G) \rightarrow [0,1]^2,$$

representing vertex positions on the unit square.

This definition diverges from the usual notion of a geometric graph, which determines the existence of edges only between nodes within a spatial distance x in a specified norm (Penrose 2003). Moreover, geometric graphs are usually only discussed in the context of random graph models, a concept first introduced by Gilbert (1961). Denote the set of geometric graphs with n edges by G_Φ^n . The spatial embedding of

geometric graphs allows us to define (random) connectivity depending on vertex positions and inter-vertex distances. Central to this study is the distance-dependent random graph model, in which edges are added with probability $p(x)$ depending on the distance x between vertex pairs:

Definition 3.12 (Distance-dependent random graph model). Let $n \in \mathbb{N}$ and $C : [0, \sqrt{2}] \rightarrow [0, 1]$ a continuous map. A *distance-dependent geometric random graph model* $G_\Phi(n, C)$ is a random graph model over G_Φ^n , generated by distributing uniformly at random the n vertices on the unit square and adding an edge from v to w for each vertex pair $(v, w) \in V(G_\Phi)^2 \setminus \Delta_{V(G_\Phi)}$ with a probability $C(x)$, depending on the distance $x = \|\Phi(v) - \Phi(w)\|$ between the vertices.

We call the function C the graph's *distance-dependent connection probability profile*. Note that the connection profile is *not* a probability density but gives a probability of connection between a vertex pair at distance x . Clearly, connectivity statistics in the distance-dependent graph model intrinsically depend on the choice of C . To develop a thorough understanding of connectivity in the model however, mapping the distribution of inter-vertex distances is equally important. Here we calculate the distribution of the distance between two random points in a square of side-length s . Being able to identify distributions of transformed random variables is integral to the calculation:

Lemma 3.13. *Let X, Y be independent continuous random variables with values in \mathbb{R} , denote with f_X and f_Y their probability distribution functions.*

- (1) *The distribution of the random variable $X + Y$ is given by the probability density function*

$$f_{X+Y}(x) = \int_{\mathbb{R}} f_X(z)f_Y(z-x) dz.$$

- (2) *The distribution of the random variable X^2 is given by the probability density function*

$$f_{X^2}(x) = \begin{cases} \frac{1}{2\sqrt{x}} (f_X(\sqrt{x}) + f_X(-\sqrt{x})) & x > 0 \\ 0 & x \leq 0 \end{cases}$$

- (3) *Let X only take positive values. Then the distribution of the random variable \sqrt{X} is given by the probability density function*

$$f_{\sqrt{X}}(x) = \begin{cases} 2xf_X(x^2) & x \geq 0 \\ 0 & x < 0 \end{cases}$$

Theorem 3.14. Let D be a random variable mapping to the distance of two random points in the square $[0, s]^2$ of side-length s . Then the distribution of D is given by the probability density function

$$f(x) = \begin{cases} \frac{2x^4 - 8sx^3 + 2\pi s^2 x}{s^4} & x \in [0, s] \\ \frac{H(x)}{s^4} & x \in [s, s\sqrt{2}), \\ 0 & x \notin [0, s\sqrt{2}) \end{cases} \quad (3.1)$$

where

$$H(x) = 8sx\sqrt{x^2 - s^2} - 2x^3 - 4s^2x \left(1 + \arcsin \left(1 - \frac{2s^2}{x^2} \right) \right).$$

Proof. We follow the approach described by Moltchanov (2012). Consider two independently and uniformly distributed random points $p_1 = (x_1, y_1)$ and $p_2 = (x_2, y_2)$ in $[0, s]^2$. The distance between p_1 and p_2 is given as

$$\|p_1 - p_2\| = \sqrt{(x_1 - x_2)^2 + (y_1 - y_2)^2}.$$

As a first step we calculate the distribution for $\Delta_x = x_1 - x_2$. Denote with f_{Δ_x} its probability density. Then, since $f_{-x_2}(z) = f_{x_2}(-z)$,

$$f_{\Delta_x}(d) = f_{x_1 + (-x_2)}(d) = \int_{\mathbb{R}} f_{x_1}(z) f_{x_2}(z - d) dz \quad (3.2)$$

after Lemma 3.13. Density functions for x_1 and x_2 are given by

$$f_{x_1}(z) = f_{x_2}(z) = \begin{cases} \frac{1}{s} & \text{for } z \in [0, s] \\ 0 & \text{otherwise.} \end{cases}$$

Thus we may only obtain non-zero values in (3.2) for $d \in (-s, s]$, as otherwise either one of the factors in the integrand is zero. In full we obtain the triangular distribution (Simpson 1755),

$$f_{\Delta_x}(d) = \begin{cases} 0 & d \notin (-s, s] \\ \frac{s+d}{s^2} & d \in (-s, 0] \\ \frac{s-d}{s^2} & d \in (0, s]. \end{cases}$$

Next we calculate the distribution for $\Delta_x^2 = (x_1 - x_2)^2$. Using Lemma 3.13 once again we obtain for $d > 0$

$$\begin{aligned} f_{\Delta_x^2}(d) &= \frac{1}{2\sqrt{d}} \left(f_{\Delta_x}(\sqrt{d}) + f_{\Delta_x}(-\sqrt{d}) \right) \\ &= \frac{1}{2\sqrt{d}} \left(\frac{s - \sqrt{d}}{s^2} + \frac{s + \sqrt{d}}{s^2} \right) = \frac{1}{s\sqrt{d}} - \frac{1}{s^2}, \end{aligned}$$

and $f_{\Delta_x^2}(d) = 0$ for $d \leq 0$. Note that of course, $f_{\Delta_x^2} = f_{\Delta_y^2}$ and we will refer to this density function as f_{Δ}^2 . Convolution yields again the probability density function for the sum of the random variables Δ_x^2 and Δ_y^2 ,

$$f_{\Delta_x^2 + \Delta_y^2}(d) = \int_{\mathbb{R}} f_{\Delta^2}(z) f_{\Delta^2}(d - z) dz.$$

Finally Lemma 3.13 lets us compute

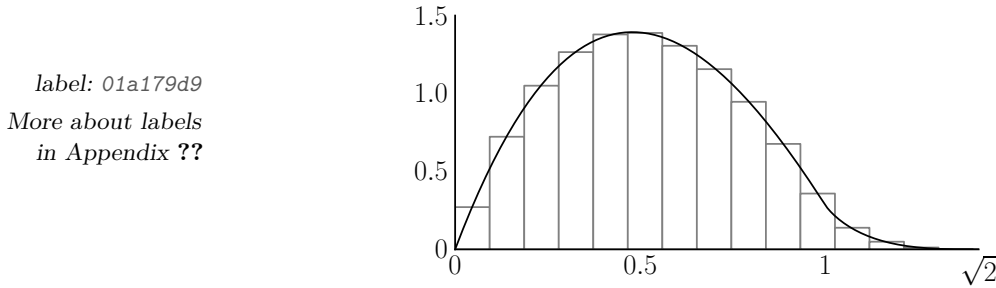
$$f_D(d) = f_{\sqrt{\Delta_x^2 + \Delta_y^2}}(d) = 2d f_{\Delta_x^2 + \Delta_y^2}(d^2),$$

for $d \geq 0$, yielding expression (3.1) for probability density function of D (Mathematica A.1, A.2). \square

The distribution for the distance between two random points in the unit square $[0, 1]^2$, is then obtained from (3.1) by setting $s = 1$. The probability density function f becomes

$$f(x) = \begin{cases} 2x^3 - 8x^2 + 2\pi x & x \in [0, 1) \\ 8x\sqrt{x^2 - 1} - 2x^3 & \\ -4x - 4x \arcsin\left(1 - \frac{2}{x^2}\right) & x \in [1, \sqrt{2}) \end{cases} \quad (3.3)$$

Plotting f in combination with the results of a numerical simulation (10000 points randomly distributed on unit square, extracted distances binned to a of width $\sqrt{2}/15$) verifies our calculation:



Density functions 3.1 and 3.3 are of high importance. Here we use 3.3 to compute the probability that a random pair of vertices in the distance-dependent random graph model is connected:

Corollary 3.15. *Let $v \neq w$ be vertices in an arbitrary realization of $G_{\Phi}(n, C)$. The probability p for an edge from v to w is given by*

$$p = \int_0^{\sqrt{2}} C(x) f(x) dx,$$

where $f(x)$ is the probability density function (3.3).

Example Let $C(x) = 1 - \frac{x}{\sqrt{2}}$. Then we compute the probability to find an edge between a random vertex pair in $G_\Phi(n, C)$ according to Theorem 3.15 as

$$p = \int_0^{\sqrt{2}} f(x) dx - \frac{1}{\sqrt{2}} \int_0^{\sqrt{2}} x f_D(x) dx = 1 - \frac{1}{\sqrt{2}} \mathbf{E}[D].$$

The expected distance between two random points on the unit square is computed as $\mathbf{E}[D] \approx 0.521405$ (Mathematica A.1), a result confirmed by Philip (2007). Thus we obtain the probability for connection of $p \approx 0.631311$

?? TODO: Subgraphs and motifs!! (remember index)

4

NETWORK MODEL

Motivated by anisotropic characteristics in connectivity in local cortical circuits found in the rat’s brain, a network model with anisotropic tissue geometry is developed. Employing both a graph theoretic definition and a numerical implementation, distance-dependent connectivity present in the model is exposed. The introduction of a rewiring algorithm and quantitative anisotropy measure lays the foundation for the analysis of structural aspects of the anisotropic network model in Chapter 5.

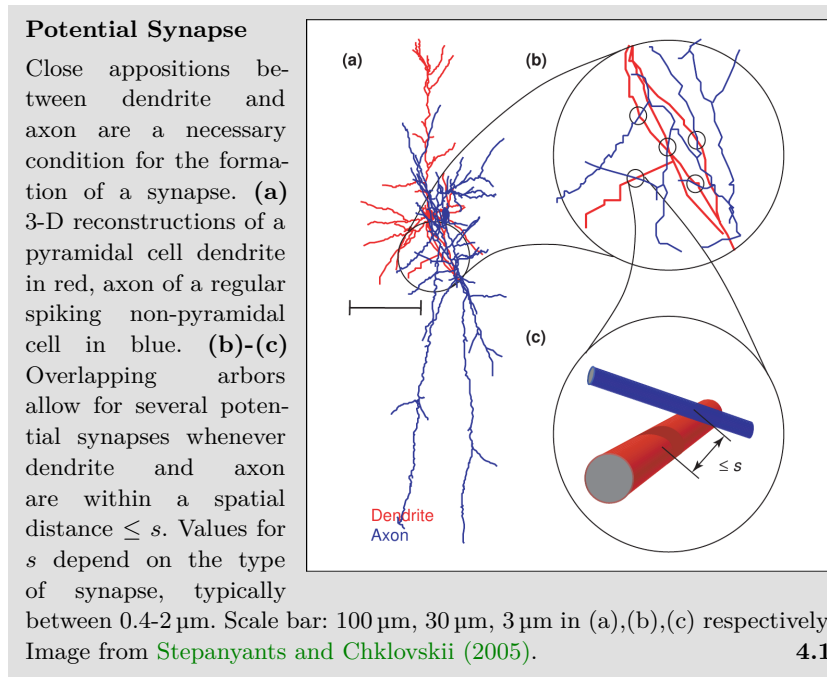
4.1 OVERVIEW

This chapter introduces the central object of this study, the *anisotropic network model*. Reviewing connectivity in local cortical circuits in Section 4.2, we identify anisotropy in connectivity in layer V pyramidal cells, inferred by their specific neuronal anatomy. Reducing the complex neuron morphology to characteristic axonal and dendritic profiles, we introduce the anisotropic network model in Section 4.3. While a graph theoretic definition allows for analytical considerations, a numerical implementation enables us not only to support the analytical observations but also gives access to results that go beyond. To fully harness this implementation we argue for the choice of a specific parameter set in Section 4.4, allowing us to generate a set of “sample graphs” to which we will refer through this study.

Using the analytical and numerical approach in conjunction, in our analysis of anisotropic networks we are most interested in identifying structural aspects that are due to the network’s anisotropy in connectivity and do not occur in similar, isotropic networks. To be able to make this distinction, in Section 4.5 we extract the distance-dependent connectivity of anisotropic networks, as it is imposed by the specific geometric relations present in the network. We then go on to introduce “rewiring” in Section 4.6, a method that allows us to manipulate the anisotropic networks to eventually display isotropy in connectivity. Finally then, Section 4.7 ties together the previous concepts by providing a measure for anisotropy and showing how rewiring is, in fact, providing the transition from anisotropic networks to networks with isotropy in connectivity.

4.2 ANISOTROPY IN NEURAL CONNECTIVITY

Neurogeometry addresses the problem of inferring synaptic connectivity from the geometric shapes of axon and dendrites. A fundamental concept in this field is that of a *potential synapse* (Stepanyants et al. 2002). Defined as the potential axonal-dendritic connection of two neurons, present whenever the axon of one neuron is within a spatial distance s of the dendrite of the other, it is a necessary, although not sufficient, condition for the formation of a synaptic connection (Figure 4.1). The existence of such close appositions solely depends on dendritic and axonal anatomy; identification of defining morphological characteristics in both axon and dendrite would therefore allow for a model of local network connectivity, assuming for example that a certain ratio r of potential synapses turn into active contacts independently. It is the hope that such a model, motivated from the geometry of a neuron's functional compartments, not only displays inherent patterns of connectivity similar to what has been observed in biological networks, but also proofs itself as a testing ground for how this connectivity may affect network dynamics.



high variability in
axonal
morphology

Finding stereotypical anatomical characteristics however is difficult, as axonal morphology is, in general, highly diverse (Debanne 2004). Across different species, distinct regions in the central nervous system and different neuron types, axons display a wide variety of shapes characterized by morphometric parameters such as total length, branching complexity and axonal extent (Ropireddy et al. 2011). Typical exam-

ples of distinct morphology include the T-shaped axons of cerebellar granule cells branching only at a singular point (Ramon and Cajal 1911), and axons of hippocampal CA3 pyramidal cells, which, in stark contrast, may feature up to 40 branches resulting in a total length of axon collaterals of up to 12 mm (Ishizuka et al. 1990).

It is therefore imperative to confine this analysis to a specific brain region and neuron type. In this study, we set the focus on circuits of pyramidal cells in the mammalian cortex. More specifically, local circuits of thick tufted layer 5 pyramidal neurons in the rat's somatosensory cortex have been the target of advanced experimentation (Song et al. 2005; Perin et al. 2011; Romand et al. 2011; Ramaswamy et al. 2012), and will serve as a benchmark for results in neural morphology and network connectivity in this report.

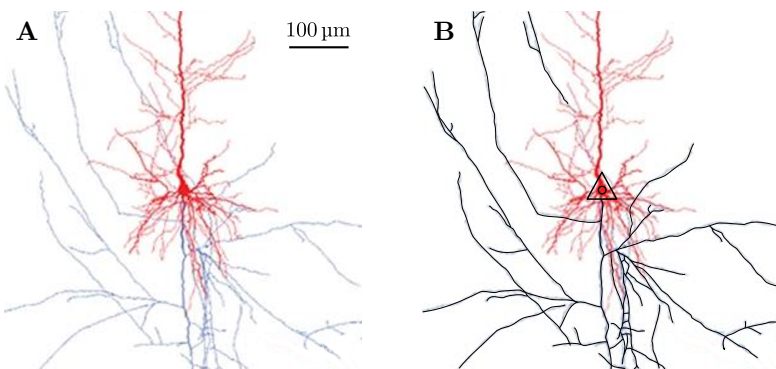


Figure 4.2: Tracing axonal branching of a pyramidal cell In a 3-D model reconstructed from biocytin-labeled thick-tufted layer 5 pyramidal cells in the somatosensory cortex of postnatal (day 14) Wistar rats, Romand et al. (2011) depict dendritic compartments in red, axonal compartments in blue. **A)** A 600 μm window centered on the soma of the pyramidal cell shows the main stem of the cell's axon projecting downwards in a straight line, collaterals branching at various angles. **B)** Using image manipulation software, axon morphology was manually traced and is emphasized in black.

Axonal morphology of pyramidal cells in the cerebral cortex is well described. From the soma the single main stem of the axon originates and projects downwards, describing a trajectory closely resembling a straight line (Braitenberg and Schüz 1998). At arbitrary points along this path, collaterals branch off at various angles and constitute themselves linear paths until they further ramify or terminate. Displaying a high degree of ramification, axonal trees of cortical pyramidal cells build, in general, complex structures (Petersen et al. 2003; Ramaswamy et al. 2012). Cortical slice experiments analyzing neural anatomy are typically constrained by a slice thickness of 300 μm . On this scale, 3-D reconstruction from labeled thick tufted layer 5 pyramidal cells reveals

cortical axons
form straight lines,
arborize profusely

characteristic morphology of the axonal tree (Figure 4.2). The downwards projecting, straight axon branches at several points, forming collateral branches that travel in linear path as well.

In a statistical view, this characteristic axonal morphology results in high axon branch densities along the main stem, whereas distant regions display a relatively low density (Figure 4.3). Specifically, axon collaterals do not cluster around the soma but align with the main stem's projection. As presence of an axonal branch constitutes a necessary condition for a potential synapse, a higher concentration of potential and, subsequently, realized synapses is expected in regions of high branch density. For a coherent picture of local connectivity profiles, however, dendritic morphology needs to be considered as well.

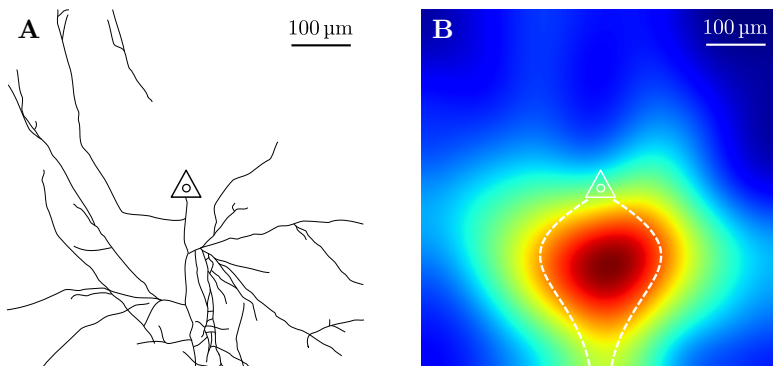


Figure 4.3: Illustrating axonal branch density In a sample of 5 reconstructions from thick-tufted layer 5 pyramidal cells (Romand et al. 2011), tracing axonal morphology illustrates characteristic branch density along the axon's main stem. **A)** Example of extracted axonal tree. Outline manually traced using image manipulation software. Soma indicated by triangle. Original data from Romand et al. (2011). **B)** Overlaying 5 axonal trees extracted as in A), applying a Gaussian filter and displaying high axon densities in warm colors, illustrates the characteristic higher branch densities along the axon's main stem.

basal dendrites dominate local connectivity

Dendritic anatomy of cortical pyramidal cells is inherently bipartite. From the soma several *basal dendrites* emerge and extend into arbitrary directions, branching profusely until they terminate. The single *apical dendrite* emerges from the apex of the pyramidal cell and ascends in a linear trajectory, forming occasional collateral branches until finally terminating into the apical tuft, where the dendrite branches several times to form a tree like structure (Feldman 1984). On the scale of typical cortical slice thickness, however, the apical dendrite is cut off and the basal dendrite dominates the dendritic morphology and potential of dendritic-axonal connections (Figure 4.4). The radial extension of dendritic branches results in a high concentration of dendritic branches

around the soma, much in the contrast to the findings of axonal branch densities before.

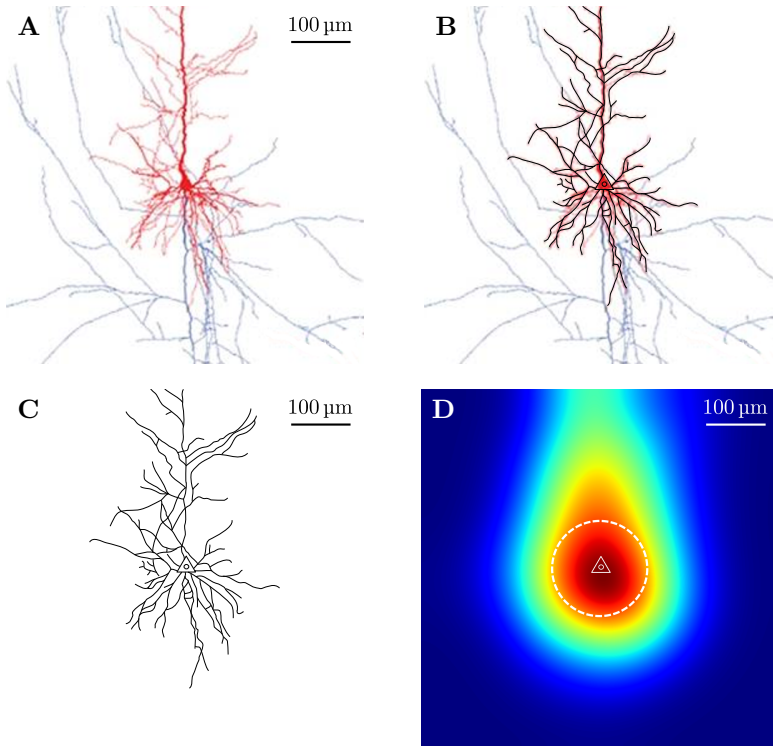


Figure 4.4: Dendritic morphology and branch density Using neuronal morphology of thick-tufted layer 5 pyramidal cells recorded by Romand et al. (2011), dendritic anatomy is traced and combined to illustrate high branch density around the soma. **A)** In a 600 μm window centered on the soma, basal dendrites (red) are visible extending around the soma. The ascending thick apical dendrite (red) is cut off and apical tuft is not shown. **B)-C)** Manual tracing of dendritic outlines in five samples (one shown), allows for clearer identification of stereotypical morphology and later analysis. **D)** Combining 5 dendritic outlines as shown in C) and subsequent Gaussian filtering reveals the relatively high dendritic branch density around the soma.

Combining the above results of dendritic and axonal branch densities in the light of neurogeometry, a clear concept of anisotropy of neural connectivity emerges. As dendritic branches of potential post-synaptic targets extend radially from the soma and do not display a preferred direction, target neurons for outgoing synaptic contacts originating from a single pyramidal cell, cluster around the downwards projecting axon (Figure 4.5). In their in-depth study, Stepanyants and Chklovskii (2005) confirm the overrepresentation of potential synapses along the axon for pyramidal cells. Consistent with the notion that stereotypical morphology of pyramidal cells is intrinsic to the local network's connectivity

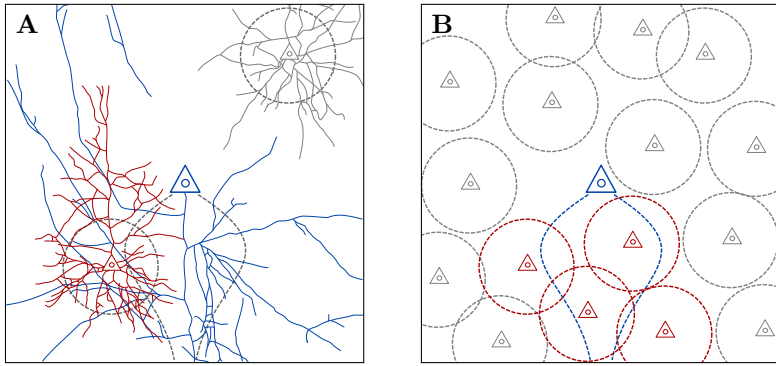


Figure 4.5: Connected neurons of a single pyramidal cell align with axonal projection Reducing the full axonal (blue, cf. Figure 4.2) and dendritic trees (red, gray, cf. Figure 4.4) as shown for two neurons in A) to their stereotypical axonal (blue) and dendritic profiles (red, gray) in B), demonstrates how connected neurons (red) tend to cluster around the pre-synaptic axon's profile, as spatial closeness constitutes a necessary condition for the formation of contacts. Unconnected neurons (gray) are found distant from the axon's projection, but not necessarily distant from the soma.

profile, they also find that anisotropy of this degree is *not* present in spiny stellate neurons located in lower-layer-4.

4.3 ANISOTROPIC GEOMETRIC NETWORK MODEL

Taking up the concept of anisotropy in neural connectivity introduced in the last section, we propose here, as basis for this study, a simple geometric network model featuring anisotropic connectivity. Constructing such a model, we're challenged with resembling the anisotropic aspects outlined last section as closely as possible, while at the same time basing the model on simple and abstract relations to allow for an analytical study of such anisotropic networks.

With this in mind, we propose the following model: On a square surface of side length s , a number of N point neurons are randomly, uniformly distributed. Connected neighbors are then calculated for each neuron separately and independently, by determining the randomly, uniformly distributed direction of the neuron's single axon. In this direction the axon traverses over the surface describing a straight path, terminating only when an edge of the surface is reached. Directed contacts are made with every neuron that is within a width $w(x)$ of the axon's trajectory, where in general w depends on the axon length x at this point (Figure 4.6).

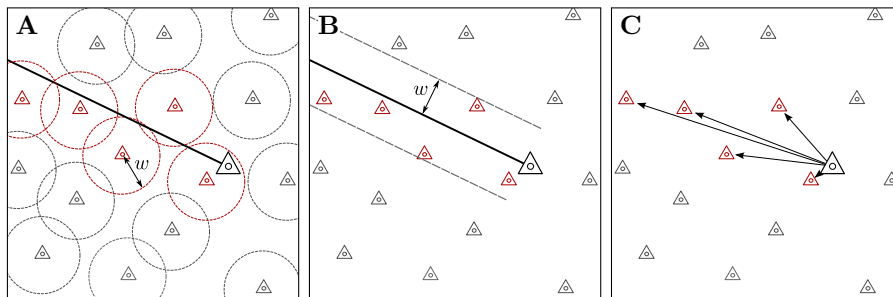


Figure 4.6: Anisotropic geometric network model and interpretations of width parameter w Illustrating the process of finding connections for one neuron (large triangle, black), the axon describes a linear trajectory in an arbitrary direction and until terminating on the surface's edge. Target neurons (red) are encountered along the path within a (here constant) distance w , which is in **A**) interpreted as a dendritic radius or, equivalently, in **B**) as a “bandwidth” of the axon. Connections to the encountered targets are then established as projections in **C**), consistent with the directed nature of synapses in biological networks (cf. Chapter 2).

The implementation of arbitrary axonal orientation is crucial to the model. Although cortical axons are described as consistently projecting downwards (Braitenberg and Schüz 1998, cf. Section 4.2), combining exclusively vertically aligned axons with the simplified axonal and dendritic morphological profiles would result in a “vertically staggered

random axonal orientation yields relevant connectivity

connectivity" - neurons could then only project to targets located below them. It is in fact not a vertical alignment of axon orientation, but the anisotropy in neural connectivity - the observation of neuronal targets aligning with the axonal projection - that we try to capture and analyze in this model.

We will refer to the model as the *anisotropic geometric network model*. Trying to provide a simple, abstract model isolating anisotropy in connectivity, in most of this study the width $w(x)$ is assumed to be constant, $w(x) = w$, a notable exception being the development of tuned networks in Section 5.5. In the graph theoretic context the anisotropic network model is a random graph model, in which a realization of the random process results in a geometric directed graph with a special mode of connectivity. We can formally define such realization as:

Definition 4.1 (Anisotropic geometric graph). Let $n \in \mathbb{N}$ and $w \in (0, \infty)$. An *anisotropic geometric graph* $G_{n,w}$ then consists of a tuple (G, Φ, a) , of a simple directed graph G with $|V(G)| = n$ vertices and the maps $\Phi : V(G) \rightarrow [0, 1]^2$ and $a : V(G) \rightarrow [0, 2\pi)$, such that for every vertex pair $v, v' \in V(G)$ and edge $e \in E(G)$ with $s(e) = v$ and $t(e) = v'$ exists if and only if the inequalities

$$R_{-a(v)} (\Phi(v') - \Phi(v)) \hat{e}_x \geq 0 \quad \text{and} \quad \left| R_{-a(v)} (\Phi(v') - \Phi(v)) \hat{e}_y \right| \leq \frac{w}{2}$$

hold. Here R_φ is the rotation matrix of angle φ in the Cartesian plane and \hat{e}_x, \hat{e}_y are the standard unit vectors.

The anisotropic random graph model then is then giving the probability distribution over the set of anisotropic random graphs by describing a random process generating such graph.

Definition 4.2 (Anisotropic random graph model). Let $n \in \mathbb{N}$ and $w > 0$. The *anisotropic random graph model* $G(n, w)$ is a probability space over the set of anisotropic geometric graphs with a probability distribution induced by the following process: Let G be an empty graph with n vertices. Assign randomly and uniformly to every vertex $v \in V(G)$ a position $\Phi(v) \in [0, 1]^2$ and axonal orientation $0 \leq a(v) < 2\pi$. Then add edges such that (G, Φ, a) is an anisotropic geometric graph $G_{n,w}$.

*anisotropic model
is scale-free*

As with every geometric graph model introduced, we restrict the surface to be the unit square. This does not limit the model, as only the relative width of the axon band in regard to the surface's side length is determining connectivity statistics - the expected number of connections is easily obtained by the quotient of the area covered by the axon and the surface area, making connectivity statistics in the anisotropic random graph model scale-free.

The following maybe interpreted as a study of anisotropic geometric graphs in the light of a neuroscientific context. To enable such an analysis, a few more concepts are needed. The introduction of those concepts composes the rest of the chapter. A first important step is the numerical implementation of the anisotropic network model.

4.4 NUMERICAL IMPLEMENTATION

Numerical implementation of the anisotropic random graph model was achieved in Python¹. Relying on NumPy as part of the scientific Python library SciPy² for the more complex mathematical computations, the implementation also uses graph-tool³, to ensure convenient and efficient handling of the created networks.

The algorithm for the generation of anisotropic networks closely resembles Definition 4.1. After randomly distributing N neurons on the square of side-length s , for every neuron a random axon orientation $a \in [0, 2\pi)$ is chosen and an affine transformation, such that the current neuron is located at the origin and its axon projection aligns with the positive x-axis, secures a straightforward implementation of connectivity, using the the inequalities in Definition 4.1 as a rule for establishing connections.

To harness the numerical implemenation to generate networks, a set of parameters needs to be chosen. The network size N strongly influences the needed computational efforts in calculations based on the generated graphs and has thus been set to $N = 1000$. Choosing the surface side-length arbitrarily as $s = 100$, the axon width w determines connectivity in the network, the relation between width w and overall connection probability p being shown in Figure 4.7. In their analysis of connectivity of thick-tufted layer 5 pyramidal cells in neonatal rats (day 14), Song et al. (2005) report an overall connection probability of $p = 0.116$, consistent with prior reports of a cortical connection probability of $p \approx 0.1$. Choosing w to be constant, we determine the axon width such that overall connectivity matches the value report by Song et al. and obtain $w/2 = 12.6$ (Figure 4.7).

*parameter set
chosen to resemble
cortical circuits*

Having determined a suitable set of parameters as $N = 1000$, $s = 100$ and $w = 25.2$, we generate 25 graphs with this parameter set

¹ Python Software Foundation. Python Language Reference, version 2.7. Available at <http://www.python.org>

² Eric Jones, Travis Oliphant, Pearu Peterson and others. NumPy version 1.6.1. Available at <http://www.scipy.org>

³ Tiago P. Peixoto. Efficient network analysis. Version 2.2.18. Available at <http://graph-tool.skewed.de/>

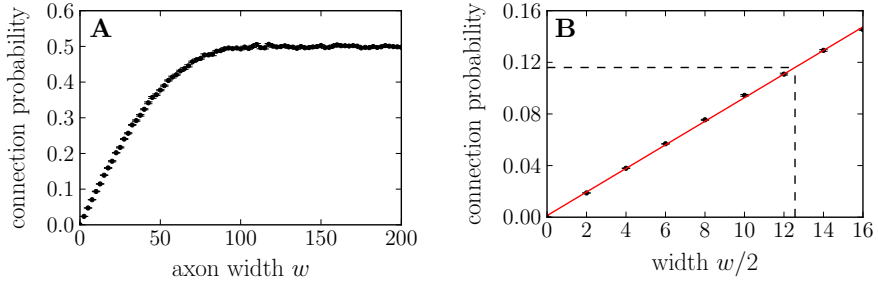


Figure 4.7: Axon width dependent connection probability determines parameter for numerical analysis Generating anisotropic networks with different axon widths w and extracting probability p of directed connection between two random nodes, demonstrates the dependency of p on the width parameter w . **A)** At an axon width of over $w = 100$, exceeding the square's side length, the connection probability saturates at $p = 0.5$, as axon bands are essentially “cutting” the square in a connected and unconnected half (c5b64f3e). **B)** For small w the connection probability is a linear function of w , allowing the width $w_S/2$ at which $p(w_S) = 0.116$ to be determined by a linear fit as $w_S/2 = 12.6$ (585a946f).

sample graphs as
reference for
structural analysis

(label: N1000w_ax126-flat_graph0-24). This set of sample graphs will serve as a reference for the following structural analysis. Extending the set by the (partially) rewired sample graphs (see Section 4.6) and by purely distance-dependent graphs best resembling the anisotropic networks (see Section 4.5) we obtain a resourceful reference for the analysis of structural features of anisotropic geometric graphs, that we will frequently employ to obtain quantitative and qualitative results.

4.5 DISTANCE DEPENDENT CONNECTIVITY

In Gilbert's random graph model $G(n, p)$, probability of connection p is independently chosen and a fixed value for all vertex pairs. The anisotropic geometric graph model introduced in Section 4.3 is itself a random graph model - node positions as well as preferred directions of connection are uniformly at random distributed. In contrast to Gilbert's model however, neither is the probability of connection between a given vertex pair independent of the realization of other edges in the graph, nor is it a fixed value - probabilities strongly depend on internode distance in the anisotropic geometric graph model introduced.

*random graph
models in
Section 3.3*

Analyzing dependencies in the anisotropic model, specifically by identifying prevalent patterns of connectivity and relating these modes of non-randomness to biological findings, is the main focus of Chapter 5. However, such structural correlations may not necessarily be an inherent feature of the network's anisotropy - distance dependent connectivity alone, as imposed by the model's specific geometry, may be the cause for emerging dependencies. It is therefore a crucial initial task to map the anisotropic model's distance dependent connection probability. Inferring connection probability as a function of internode distance and comparing it with computational results, in this section we explore distance connectivity of the anisotropic network model, securing a vital component in the analysis of structural features.

Theorem 4.3. *Let (G, Φ, a) represent an arbitrary realization of the anisotropic random graph model $G(n, w)$. Define $C : [0, \sqrt{2}] \rightarrow [0, 1]$ as the distance-dependent connection probability profile of (G, Φ) , that is such that $C(x)$ is the probability that for a vertex pair $(v, v') \in V(G)^2 \setminus \Delta_{V(G)}$ in distance $x = \|\Phi(v) - \Phi(v')\|$ the vertex v projects to vertex v' . Then*

$$C(x) = \begin{cases} \frac{1}{2} & \text{for } x \leq w/2 \\ \frac{1}{\pi} \arcsin\left(\frac{w}{2x}\right) & \text{for } x > w/2. \end{cases}$$

Proof. Let v, v' be a pair of vertices in $V(G)^2 \setminus \Delta_{V(G)}$ in Euclidean distance x of each other. The vector difference $\Phi(v') - \Phi(v)$ may then be written as $xe^{i\theta}$, with $0 \leq \theta < 2\pi$. We have

$$R_{-\alpha(v)} xe^{i\theta} = xe^{i(\theta - \alpha(v))}.$$

Only for suitable combination of θ and $\alpha(v)$ an edge from v to v' exists. Assuming $\alpha(v)$ fixed, we calculate the probability of connection depending on the random choice of θ . We can assume $\alpha(v) = 0$, otherwise the same argument holds for $\theta' = \theta - \alpha(v)$.

From 4.1 we obtain the necessary and sufficient conditions

$$x \cos \theta \geq 0 \quad \text{and} \quad |x \sin \theta| \leq \frac{w}{2}.$$

Choosing uniformly at random θ in the range of $[0, 2\pi)$, the first condition is satisfied with a probability of $\frac{1}{2}$. Consider for the second condition $\theta \in [0, \pi)$. We have

$$\sin \theta \leq \frac{w}{2x},$$

and for $x \leq \frac{w}{2}$ the inequality holds for all θ by definition of $\sin \theta$. In the case of $x > \frac{w}{2}$, we note that for the first condition to hold θ must already be in $[0, \frac{\pi}{2})$ and can thus write the second condition θ as

$$\theta \leq \arcsin \frac{w}{2x},$$

yielding $C(x)$ by combining the considerations above and using the symmetry of sine for θ in the third and fourth quadrant. \square

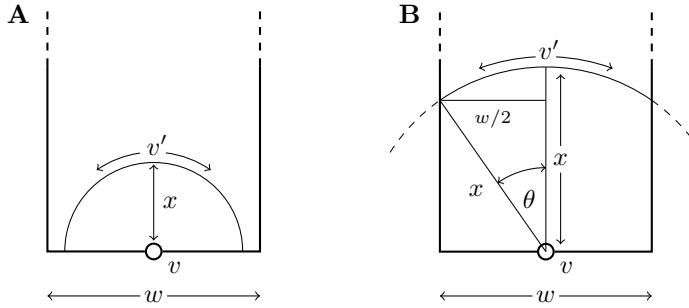


Figure 4.8: Illustrating the proof of Theorem 4.3 Distance-dependent connectivity profile $C(x)$ in an anisotropic geometric graph calculated from geometric dependencies. **A)** In the case of $x \leq w/2$, target v' may be located anywhere on the shown semicircle and therefore receives input from v with probability $1/2$. **B)** For $x > w/2$, suitable positions for target v' are dependent on x . The geometric relation $\sin \theta = w/2x$ leads to the distance-dependent connectivity profile as described in Theorem 4.3.

distance-dependent sample graphs as reference

We can verify this result by extracting the distance-dependent connection probabilities in the sample graphs created in Section 4.4. Combining data of all 25 graphs, we find that connection probabilities perfectly match the theoretical prediction (Figure 4.9). Additionally we're able to extend the reference sample graphs by distance-dependent networks (Definition 3.12). Using Theorem 4.3 in conjunction with the sample graph parameter set ($N = 1000$, $s = 100^4$, $w = 25.2$) we easily obtain the expected distance-dependent connectivity profile for the

⁴ The generalization of Theorem 4.3 to allow for arbitrary side-length s is trivial and omitted here

created sample graphs and, using this profile, generate purely distance-dependent networks⁵. Being highly interested in structural features not explained by distance-dependent connectivity, the numerical analysis in this work will heavily rely on these networks to identify aspects that are inherent to the anisotropy in connectivity.

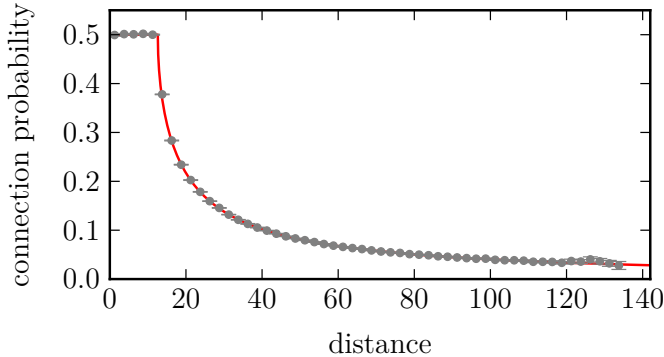


Figure 4.9: Predicted distance-dependent connection probability profile is matched by numerical results Averaging distance-dependent connection probabilities over the 25 sample graphs, we find the expected profile calculated in Theorem 4.3 is matched perfectly by the numerical results. (dbffa88e)

4.6 REWIRING

Distance-dependency as identified in the last section may already account for many of the structural features present in anisotropic networks. A central question of this study is: What structural aspects in the network are truly features of the anisotropy in connectivity? Although a quantitative measure for anisotropy will only be introduced in the next section, already here we are able to qualitatively observe the strong directionality in connectivity - edges originating from one node “point in the same direction”, effectively aligning with the orientation of the axonal projection of the source node (cf. Figure 4.6). To answer the question above, we need to introduce a method that eliminates this directionality, making networks essentially isotropic in connectivity. Then, structural features present in the original anisotropic networks, but not in their rewired, isotropic counterparts may be attributed to anisotropy.

*eliminate
anisotropy to find
structures caused
by it*

Rewiring as introduced here, provides the transition from anisotropic connectivity to networks isotropic in connectivity, closely resembling purely distance-dependent networks. Applying this process only partially then allows us to analyse structural features as they change with

⁵ label: N1000-dist_depend-flat_graph-00-24.xml.gz

a varying degree of isotropy, asserting the importance of this process to our study. In designing the specific rewiring algorithm we identify two requirements that our implementation should satisfy:

1. elimination of anisotropy in connectivity
2. preservation of distance-dependent connectivity

The second point is especially important to us, as we want to impose isotropy on the network at “minimal cost”, that is by changing as little as possible about the other characteristics of the network’s connectivity. The following process respects both of the points above:

For every edge between vertices v and v' with inter-vertex distance x , identify neurons with distance to v in the range of $(x - \varepsilon, x + \varepsilon)$ as potential new targets. Then pick at random one of these vertices (including v') as a new target for the current edge, if such an edge doesn’t already exist ([Figure 4.10](#)).

In the graph theoretic context we formally define a rewiring as follows:

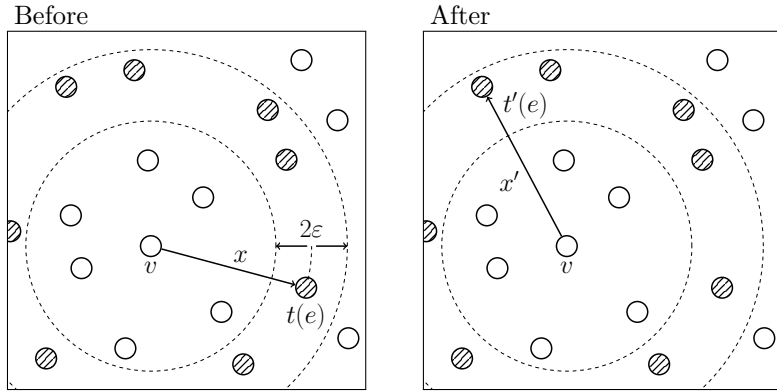


Figure 4.10: Rewiring transforms anisotropic geometric graphs to networks with isotropic connectivity For a given edge e with a distance x from its source vertex v to its target vertex $t(e)$, potential new targets (striped) are found in within a distance $(x - \varepsilon, x + \varepsilon)$ of v . The rewired edge then projects from v to a new target $t'(e)$, randomly chosen from the set of vertices within in this range. Inter-vertex distance between v and $t'(e)$ differs by less than ε from x , ensuring that for small ε the original distance-dependent connectivity is preserved. (Note that all targets within range are eligible for rewiring as no other edges exist. In general this is not the case.)

Definition 4.4. Let G be an anisotropic geometric graph with $|V(G)| = n$ and $\varepsilon > 0$. Then we define a *rewiring* R_ε of G to be probability space over G_Φ^n , induced by the following process: For every edge $e \in E(G)$

uniformly at random pick a potential new target $t'(e)$ from the set $M_e = T_e \setminus K_e$, where T_e is the set of all vertices that differ in their distance to $s(e)$ less than ε from the distance of $s(e)$ to $t(e)$,

$$T_e = \{v \in V(G) \setminus s(e) \mid |\text{d}(s(e), v) - \text{d}(s(e), t(e))| < \varepsilon\}$$

and K_e the set vertices that already are connected to $s(e)$ by another rewired edge,

$$K_e = \{v \in V(G) \mid \exists e' \in E'(G) : s(e') = s(e), t(e') = v\},$$

where $E'(G)$ is the set of all edges that have been rewired already.

Note that in the way Definition 4.4 is formulated, it is possible for M_e to be empty for some edge e . In this case no new edge is realized and the resulting, rewired network has $|E(G)| - 1$ edges. In practice this happens negligibly seldom, out of approximately on average only 25.68 edges, with a standard deviation of 4.51 and accounting for roughly 0.02% of the rewired edges, are “lost” in this process (4afc2727).

We formulated Definition 4.4 in such a way, that distance-dependent connectivity is preserved. We verify this claim by the following estimation:

Let $\tilde{C}(x)$ be the distance-dependent connectivity profile of a rewiring R_ε of an anisotropic graph $G_{n,w}$. Denote with $C(x)$ the distance-dependent connection probability of the $G_{n,w}$. The expected value for $\tilde{C}(x)$ at any inter-vertex distance $x \in [0, \sqrt{2}]$ is given as an average over the connection probabilities $C(x)$ of the possible sources to the new edge at distance x

$$\mathbf{E} [\tilde{C}(x)] = \frac{1}{2\varepsilon} \int_{x-\varepsilon}^{x+\varepsilon} C(x') dx'.$$

Note that for this expression to be well defined in the boundary cases, we need to extend $C(x)$ to have $C(x) = 0$ for $x < 0$ and $x > \sqrt{2}$. We can then estimate the expected difference between $\tilde{C}(x)$ and $C(x)$ at any point x as

$$\begin{aligned} |\mathbf{E} [\tilde{C}(x) - C(x)]| &= \left| \frac{1}{2\varepsilon} \int_{x-\varepsilon}^{x+\varepsilon} C(x') - C(x) dx' \right| \\ &= \frac{1}{2\varepsilon} \left\{ \int_{x-\varepsilon}^x C(x') - C(x) dx - \int_x^{x+\varepsilon} C(x') - C(x) dx \right\} \\ &\leq \frac{1}{2\varepsilon}, \end{aligned} \tag{4.1}$$

The rewiring margin ε thus simultaneously governs how many new targets are available for each edge and how well distance-dependency is preserved. Setting $\varepsilon = 1.25$ and applying the rewiring algorithm to the 25 sample graphs, we find that distance-dependent connectivity of

$d(v, w) = \|\Phi(v) - \Phi(w)\|$
Euclidean distance
between vertices

the original graphs is matched (Figure 4.11) while at the same time ensuring that for any edge e sufficiently many new rewiring targets are available (Figure A.1).

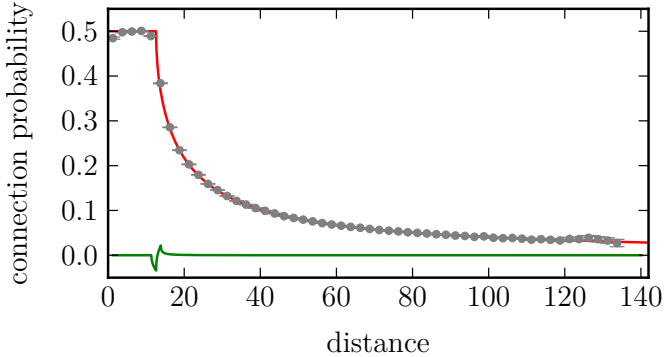


Figure 4.11: Rewiring with $\varepsilon = 1.25$ preserves distance-dependent profile in sample graphs Comparing the distance-dependent connection probabilities of the original graph (Theorem 4.3) in red with extracted of probabilities from the rewired ($\varepsilon = 1.25$) sample graphs in gray (errorbars SEM) we verify that distance-dependent connectivity is preserved when rewiring. The green curve shows the expected difference between the original and rewired distance profiles as estimated in Equation 4.1. (4f4dfcf1)

As a generalization of Definition 4.4, we define a partial rewiring $R_{\varepsilon,\eta}$, finding new targets only for a fraction η of all edges:

Definition 4.5. Let $\varepsilon > 0$ and $0 \leq \eta \leq 1$. A *partial rewiring* $R_{\varepsilon,\eta}$ of an anisotropic geometric graph $G_{n,w}$ is then a rewiring R_ε of $G_{n,w}$, in which every edge is rewired with a probability of η , otherwise it remains. To avoid the occurrence of multiple edges, K_e is then extended to include the targets of all edges originating from $s(e)$ that will not be rewired.

rewiring of sample
graphs

Clearly, as with full rewiring, partial rewiring also preserves distance-dependent connectivity. Using the algorithm we extend our set of sample graphs once more by adding rewired versions of each graph. Choosing a rewiring margin of $\varepsilon = 1.25$, with fractions $\eta = 0.25$, $\eta = 0.5$, $\eta = 0.75$ and $\eta = 1$ we obtain through rewiring five stages of the sample graphs, from complete anisotropy in connectivity in the original graphs to the isotropic, fully rewired graphs⁶. By introducing a measure for anisotropy and applying it to the rewired and original version of the sample graphs, we're able to solidify this notion and tie together the concepts introduced through this chapter in the next section.

⁶ labels: N1000w_ax126-flat_graph0-25-rewired_frac025, -50,-75,-100

4.7 ANISOTROPY MEASURE

In the last section a method to rewire an anisotropic geometric graph, such that was introduced. From an . In this chapter we introduce.. capturing ..

The $G_{n,\Phi}$ be a geometric graph. Then, for every is the *preferred direction* and its length is

Mardia and Jupp (2000)

Anisotropic model can be interpreted as a model maximizing anisotropy while keeping the cutoffs (degree distribution).

Figure 4.12: illustrate varying levels of anisotropy

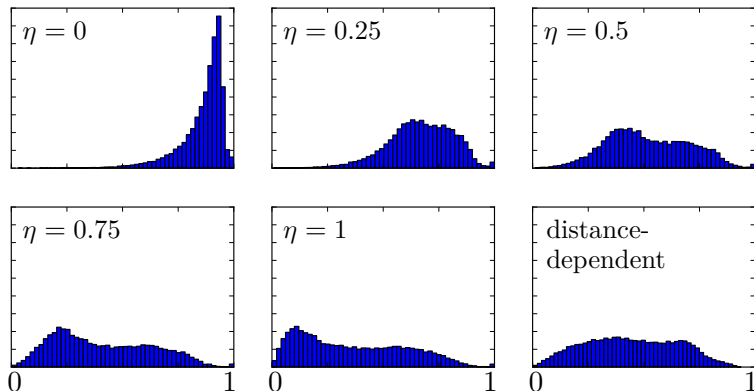


Figure 4.13: Rewiring significantly reduces anisotropy In data taken from the 25 sample graphs (Section 4.4), vertex isotropy degree distribution is shown for the original set of graphs ($\eta = 0$) The characteristic highly anisotropic profile found in the original is already significantly reduced by partial rewiring; anisotropy degree distribution in the fully rewired graphs resemble degree distribution of equivalent purely distance-dependent networks.

... suggesting that fully rewired anisotropic networks do not . There is however one difference in out-degree as an artifact of boundary confinement (Section 5.2).

4.8 SUMMARY AND DISCUSSION

has been introduced, rewiring, .

- Gilbert random graph
- distance-dependent graph
- fully rewired anisotropic graph
- anisotropic network

the claim is that distance-dependent and fully rewired are more or less equivalent (hints of non-equivalence found in ...) and so

5

STRUCTURAL ASPECTS

5.1 INTRODUCTION

Investigation of the brain's connectivity is an ongoing endeavour. Concurrent collaborative efforts like the Human Connectome Project, the Open Connectome Project and the Allen Brain Atlas, intent on mapping the 'wiring' of the brain, as well as the continued development of experimental techniques and computational resources, demonstrate the great interest in advancing this field.

Research in brain connectivity spreads over the whole scale of the brain; from the mapping of fiber pathways between brain regions at the macroscopic level, to the synaptic connections of individual neurons on the microscale, researchers are trying to identify the links that enable the brain its characteristic cognitive abilities. Connections, these links are of anatomical nature. However, statistical dependencies and causal relationships between the distinct computational units in the brain are being researched with equal emphasis ([Sporns 2007](#)).

Connectivity in the context of the anisotropic network model introduced in Section 4.3, refers in this chapter to structural links. So far, we have only briefly mentioned that the network's nodes should be interpreted as individual neurons; to allow for a discussion of functional relationships between nodes, we have yet to provided a physical description of a neuron's function. As such, we will here explore the network's structural connectivity, modeling synaptic contacts between axon and dendrites of individual neurons.

Synaptic Connectivity

In the local cortical circuits the anisotropic geometric model was derived from, synaptic connectivity is a major mode of configuration. In those networks, connectivity has been determined to be neither completely random nor exclusively specific [Source]. Recurring patterns of

HUMAN
Connectome
PROJECT

humanconnectome.org

Open Connectome
Project

[openconnectome-
project.org](http://openconnectome-project.org)

ALLEN BRAIN ATLAS

brain-map.org

connectivity have been identified by several reports (Sporns and Kötter 2004; Song et al. 2005; Perin et al. 2011).

The impact of this structural specificity discovered in local networks is shown to be significant; while the linking of network structure and network dynamics remains an active field of research, several studies were able to employ computational and theoretical models to establish such a connection. A study by Zhao et al. from 2011, for example, demonstrates how second order connectivity statistics affect a network's propensity to synchronize (Zhao et al. 2011). In the same year, Alex Roxin reported on the influence of in- and out-degree distributions on dynamics of neural network (Roxin 2011). Later, Pernice et al. were able to link structural connectivity to spike train correlations in neural networks (Pernice et al. 2011).

mapping synaptic connectivity in experiments

Experimentally, paired intracellular recordings are used to determine synaptic connectivity in cortical slices. Using two electrodes, one inserted in the cell and one outside the cell, a single intracellular recording allows for measurement of a cell's membrane potential (Brette and Destexhe 2012, Chapter 3; Weckstrom 2010). Simultaneous recordings from multiple neurons are then able to infer synaptic connectivity by evoking an action potential through current injection in one neuron and observing the change of membrane potential in the other cells (Song et al. 2005).

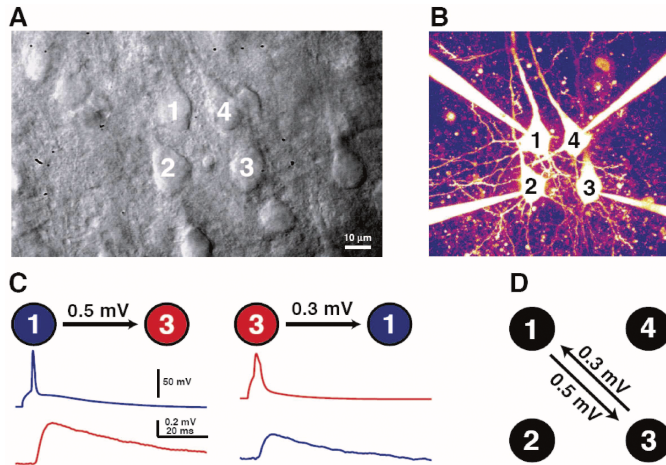


Figure 5.1: Song et al. use quadruple whole-cell recordings, observing simultaneously the membrane potential of four neurons. **A)** Contrast image showing four thick-tufted L5 neurons **B)** Fluorescent image of the same cells after patching on **C)** Evoking an action potential in the presynaptic neuron causes characteristic membrane potential change in the postsynaptic neuron **D)** Inferring synaptic connectivity from the EPSP waveform observed in C). Image from (Song et al. 2005).

While techniques for paired intracellular recordings are rapidly developing, their ability to capture connectivity patterns of large networks is yet very limited. To this date, the connectome of *C. Elegans* remains the outstanding exception of a connectivity configuration that has been fully mapped [Source]. Even in the state-of-the-art experiment conducted by Perin et al., using a setup capable of recording up to twelve neurons simultaneously, the authors note that an investigation of degree distribution was not carried out, due to lack of sufficient data (Perin et al. 2011).

Exploiting the benefits of a geometrical model

Working with a geometrical network model and its computational implementation, such restrictions disappear; the full information about the network, in form of its connectivity matrix, is given at point in time and can be easily queried for. Experiments that may take days to perform *in vivo*, can be completed in a matter of seconds *in silico*. As such, geometrical models lend themselves to extensive examination of their structural aspects.

In trying to exploit these advantages, two approaches present themselves. One may construct a network model that extrapolates the known biological configuration; a full structural examination of these networks could possibly expose relevant patterns not yet observed. For this approach a sophisticated understanding of the biological configuration is critical. Neuron morphology, however, is difficult to describe and extract.

*Extrapolation vs.
reduction*

For this analysis we suggest a reductionist approach. Having motivated an abstract model reflecting a cortical network's directional heterogeneity, we distinguish emerging patterns of connectivity, specific to directionally heterogeneous networks, from results, that only indirectly stem from the network's anisotropy, in the hopes to be able to characterize the significance of directional heterogeneity in structural connectivity of cortical circuits.

Structural aspects of the heterogeneous model

In this chapter we subject the anisotropic network model introduced in Section 4.3 to a critical analysis of its structural aspects. General network topology, as well as specific modes and patterns of connectiv-

ity, are to be identified and laid out for comparison with findings in biological neural networks.

*employing
anisotropy
measure*

In an effort to map out structural features that can be directly associated with the network's directional heterogeneity, it is crucial to differentiate such findings from results that are only indirectly caused by the network's anisotropy. To this end, already in Section 4.7 we developed a measure to quantify the degree of anisotropy prevalent in a given network; throughout this chapter we will now frequently employ this measure to determine which structural aspects are originating from the network's heterogeneity, and which aspects are to be attributed solely to the network's distance dependency.

Accordingly, results from this investigation are categorized in two sections: The first section, 'Section 2', describes structural aspects that can not be directly attributed to the model's anisotropy. The second section, 'Section 3', then presents results that are truly features of network's directional heterogeneity.

5.2 DEGREE DISTRIBUTION

The in- and out-degree of vertex in a directed graph describes the number of incoming and outgoing connection from and to other vertices (cf. Definition 3.3). As a fundamental concept in graph and network theory, the degree distribution is integral in the categorization of networks and allows for the estimation of graph properties.

Degree distribution was shown to have strong impact on the dynamics of neuronal networks models commonly used in computational neuroscience research (Roxin 2011). Increasing in-degree variance for example could be connected to the appearance of oscillations in the network. Extracting degree distributions from biological networks however, remains a challenge as many neurons need to be tracked simultaneously to obtain enough data to confidently estimate degree distributions.

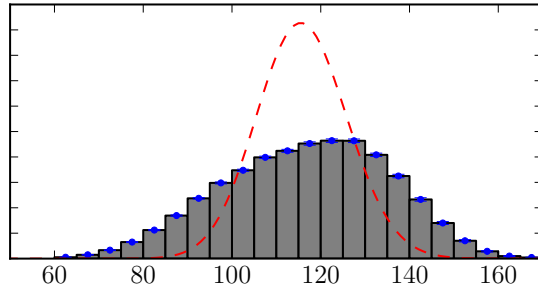


Figure 5.2: In-degree distribution in anisotropic networks shows comparably high variance and is skewed to the left From 250 anisotropic networks in-degree distributions were extracted and are shown in a normed histogram plot, errorbars SEM. Comparison with the binomial degree distribution (red) of a Gilbert random graph model with matching parameter set ($N = 1000$, $p = 0.116$) shows higher variance of in-degrees in anisotropic networks (sample variance = 344.54, variance of binomial distribution $Np(1 - p) = 102.44$.) Skewness to the left of the sample is -0.1763 . (9326138e)

Here we analyze in- and out-degrees in the anisotropic network model. First we find that compared to the binomial in-degree distribution of a Gilbert random graph model, in-degrees of vertices in anisotropic networks display higher variance and their distribution is skewed to the left (Figure 5.2). However, this specific in-degree profile is not an intrinsic property of anisotropy, as the distribution remains stable under manipulation of the anisotropy degree and closely matches the profile of a purely distance-dependent network (Figure 5.3). This result agrees with findings of Perin et al. (2011, Fig. S3), who were able to recreate

degree distributions from their experiment with layer 5 thick-tufted pyramidal cells in neonatal rats from the extracted distance-dependent connection profiles alone.

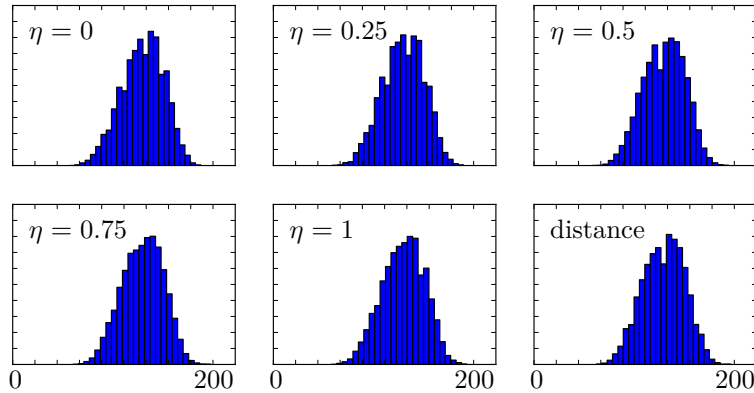


Figure 5.3: In-degree distribution not affected by varying degrees of anisotropy In-degree distributions from the 25 sample graphs and their rewiring stages are plotted in normed histograms and listed from rewiring factor $\eta = 0$ (original anisotropic) to $\eta = 1$ (completely rewired, maximal isotropy). Comparison shows that varying degrees of anisotropy do not influence the degree distribution, in fact in-degree distributions match with the degree distribution of an equivalent distance-dependent network shown bottom-right (77995b6b).

While the out-degree distribution of vertices in the anisotropic network also shows itself stable under rewiring, its distribution is drastically different from the out-degree distribution in a comparable distance-dependent network (Figure 5.4). The asymmetric, long-tailed distribution is identified as an artifact of the anisotropic network's spatial confinement; a neuron, closely located near a surface edge, might have an axon projection out of the square causing minimal out-degree or, projecting through the entire length of the surface, may have maximal out-degree. Approximating the expected number of outgoing connections for a vertex in an anisotropic network of size N , side-length s and axon width w as

$$N \frac{wl}{s^2},$$

with parameters $N = 1000$ and $\frac{w}{s} = 0.252$, we obtain an upper bound for the expected out-degree,

$$N \frac{wl}{s^2} \leq N \frac{w}{s} \sqrt{2} \approx 350.$$

If $f(l)$ is the probability density function to find axon length l for a random node v in the anisotropic network model, the out-degree distribution is then approximated by

$$\Pr[d_{\text{out}}(v) = N \frac{wl}{s^2}] = f(l), \quad (5.1)$$

see also [Figure 5.5](#).

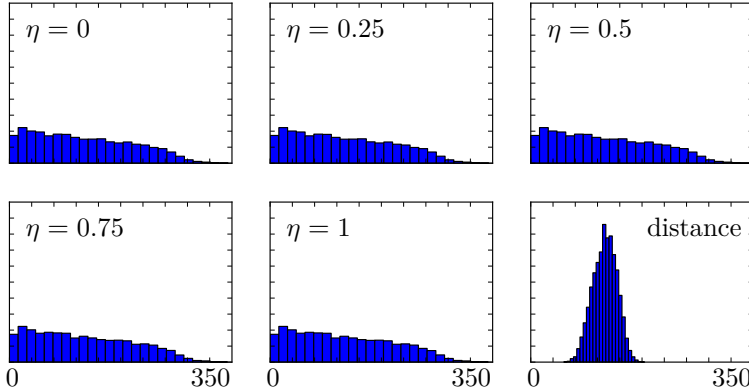


Figure 5.4: Out-degree distribution not affected by varying anisotropy but highly different from distance-dependent networks Out-degree distributions from the 25 sample graphs and their rewiring stages are plotted in normed histograms and listed from rewiring factor $\eta = 0$ (original anisotropic) to $\eta = 1$ (completely rewired, maximal isotropy). While varying degrees of anisotropy do not influence the degree distribution, the characteristic out-degree profile is drastically different from the distribution found in equivalent distance-dependent networks (77995b6b).

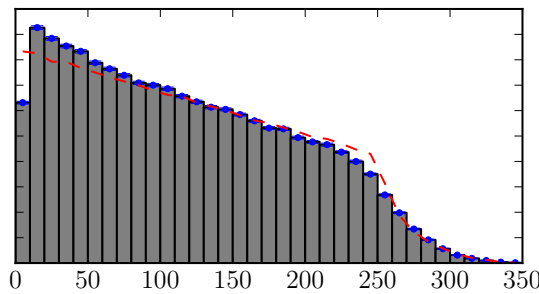


Figure 5.5: Characteristic out-degree distribution as an artifact of network's boundaries From 250 anisotropic networks out-degree distributions were extracted and are shown in a normed histogram plot, errorbars SEM. The characteristic distribution is identified as an artifact of the network's spatial confinement; using equation 5.1 the out-degree profile is approximated (red) by the distribution of axon lengths in the anisotropic network (019555b0).

5.3 SMALL WORLD PROPERTIES

Small-world networks, as described in Section 3.2, are characterized by a small average path length and comparably high clustering coefficient. In brain networks, combining advantages of sparse connectivity with mostly local and only few long-range projections, small-world properties are frequently discussed as a way of achieving high efficiency in the parallel processing of information (cf. Achard and Bullmore 2007). While most often reported on the macroscale (Sporns and Zwi 2004; Bassett and Bullmore 2006), small-worldness is also found in local cortical networks (Perin et al. 2011, SI).

*in random
networks from
independence
clustering = p*

Here we are interested in exploring the question whether anisotropy in connectivity influences the small-worldness of geometric networks. First we find that at a network size $N = 1000$, anisotropic networks display a relatively high clustering coefficient, $c = 0.1581 \pm 0.0008$ compared with $p = 0.116$ in random networks, and a comparable path length, $l_{\text{aniso}} = 1.937 \pm 0.002$ and $l_{\text{random}} = 1.8820 \pm 0.0001$, ascertaining a small-world property in the anisotropic network model.

However, is this degree of small-worldness inferred by anisotropy in connectivity? Using distance-dependent networks as a reference, we find that successively eliminating anisotropy through rewiring contributes positively to the small-world property; with rising isotropy in the network, the characteristic path length declines in small networks and remains unchanged in larger networks, while the clustering coefficient increases regardless of network size, resulting together in rewired networks to display a higher degree of small-worldness (Figure 5.6).

In distance-dependent networks the average path length is generally smaller than in (rewired) anisotropic networks (Figure A.3), matching those of a random network as reported above. At the same time also the clustering coefficient is smaller than in anisotropic networks (Figure 5.6), resulting overall in a comparable degree of small-worldness in distance-dependent networks¹ and leading to the conclusion that the observed small-worldness in the anisotropic networks is due to the imposed distant-dependent connectivity rather than the anisotropy in connectivity.

¹ Differences in the absolute values of both path length and clustering coefficient presumably relates to difference in the out-degree distribution (Figure 5.4)

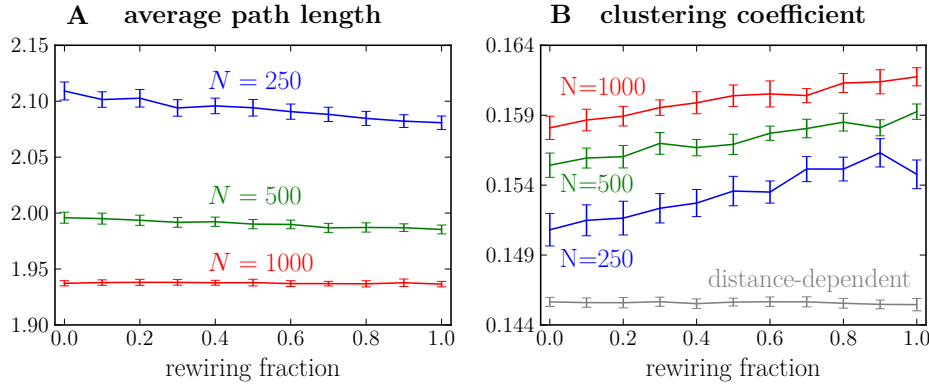


Figure 5.6: Anisotropy does not contribute to small-worldness In increasingly rewired networks, trends show a decreasing average path length and rising clustering coefficient and thus possibly a higher degree of small-worldness in the rewired, isotropically connected networks. **A)** Average path lengths for network sizes $N = 250, 500$ and 1000 , where vertex pairs with no existing are discarded. Individual value pairs are obtained by averaging over a trial size of 20, 15 and 5 respectively; errorbars are SEM. **B)** Network configuration as in A), additionally showing clustering coefficients for distance-dependent networks. (064f9b10)

5.4 TWO NEURON CONNECTIONS

Connectivity in local cortical circuits exhibits a salient feature: Examining the occurrence of connections in neuron pairs, studies have repeatedly found that bidirectionally connected neuron pairs appear much more frequently than expected from the network's overall connection probability. In layer 5 of the somatosensory cortex studies from [Markram \(1997\)](#) and [Perin et al. \(2011\)](#) have found an overrepresentation of reciprocally connected pairs of thick tufted pyramidal cells, an observation that has also been reported in layer 2/3 ([Holmgren et al. 2003](#)) and layer 5 ([Song et al. 2005](#)) of the visual cortex. The overrepresentation of bidirectionally connected pairs is significant, Song et al. for example found such pairs represented four times the expected amount.

The underlying connection principle imposing this overrepresentation on the network however remains unclear. Song et al. discuss the possibility of known learning rules to explain their findings, leaving a definitive answer open to further investigation. More recent studies find overrepresentation of reciprocally connected pairs *in vitro* resulting from functional specificity ([Ko et al. 2011](#)) and *in silico* from dense neuron clustering rules ([Klinshov et al. 2014](#)), identifying specific network characteristics that may contribute to the reported overrepresentation *in vivo*.

Here we examine anisotropy in connectivity as a possible candidate for an underlying principle explaining the characteristic two neuron connection distribution. In random networks, the chance to encounter a specific mode of connection in a random pair of neurons can easily be computed from the overall connection probability p . For this let X be the random variable of the number of edges between two different vertices in a Gilbert graph $G(n, p)$ with $n \geq 2$. As the edges are independently realized, resulting in a simple directed graph, we have

$$\begin{aligned}\mathbf{P}(X = 0) &= (1 - p)^2 && \text{unconnected pair,} \\ \mathbf{P}(X = 1) &= 2p(1 - p) && \text{single connection,} \\ \mathbf{P}(X = 2) &= p^2 && \text{reciprocal connection;}\end{aligned}\tag{5.2}$$

in short $\mathbf{P}(X = k) = \mathcal{B}_{2,p}(k)$ for $k \in \{0, 1, 2\}$ and $\mathbf{P}(X = k) = 0$ otherwise. Using this probability distribution as the expectation for connectivity of neuron pairs in the various network types, a numeric analysis of the anisotropic sample graphs reveals that bidirectionally connected pairs appear almost twice as often as expected from the overall connection probability ($p = 0.116$) and equations 5.5, similarly as reported by Song et al. (Figure 5.7 A). However, comparing the pair probabilities in anisotropic networks with the probabilities in their rewired counterparts, we find that anisotropy does not influence the occurrence of two-neuron motifs (Figure 5.7 B) In fact, expected connections in neuron pairs are identical in distance-dependent and rewired anisotropic networks (Figure A.4).

We further support this observation by computing the probability distribution for the expected number of edges between two random vertices in the anisotropic graph model. For this we assume that only the distance-dependent connection probability $C(x)$ determines the occurrence of edges in vertex pairs in the anisotropic graph model. Then, using the probability distribution $f(x)$ for the a random neuron pair to be at distance x , we calculate

$$\begin{aligned}\mathbf{P}(X = 0) &= \int_0^{\sqrt{2}} (1 - C(x))^2 f(x) dx, \\ \mathbf{P}(X = 1) &= \int_0^{\sqrt{2}} 2C(x)(1 - C(x))f(x) dx \quad \text{and} \\ \mathbf{P}(X = 2) &= \int_0^{\sqrt{2}} C(x)^2 f(x) dx.\end{aligned}$$

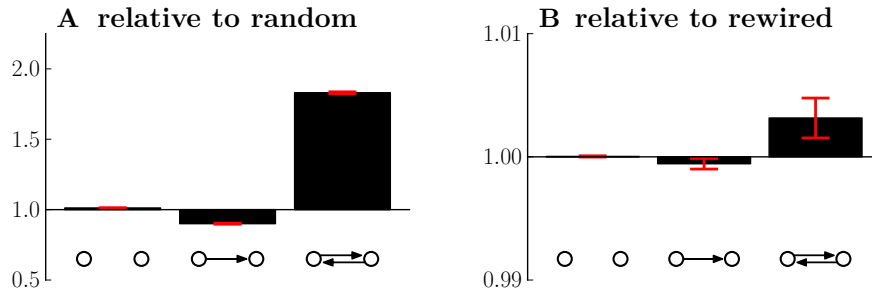


Figure 5.7: Overrepresentation of reciprocal connections in anisotropic networks due to distance-dependent connectivity Extracting the counts of unconnected, one-directionally and bidirectionally connected neuron pairs in the anisotropic sample graphs, overrepresentation of reciprocally connected pairs is identified as a feature of the network’s distance dependency as opposed to anisotropy in connectivity. **A)** Showing the quotient of the counts for the three pair types, extracted from the set of sample graphs, with the number of expected pairs in Gilbert random graphs $G(n, p)$, where $n = 1000$ and $p = 0.116$ were matched to the sample graph parameters. While single connections appear less often than in Gilbert random graphs, reciprocal connections are significantly overrepresented. Errorbars SEM. **B)** Comparing appearance of connection pairs in the anisotropic sample graphs with their respective appearance in the rewired sample graphs, we find that eliminating anisotropy does not significantly change the counts for the connection types, indicating that anisotropy does not influence two neuron connection probabilities. Errorbars SEM. (c5f1462b)

Inserting the distance-dependent connection probabilities $C(x)$ in the anisotropic graph model as computed in Theorem 4.3 and the probability distribution $f(x)$ from Theorem 3.14 we obtain

$$\begin{aligned} \mathbf{P}(X = 0) &= 0.791336 & 0.7907 \pm 0.0008 \\ \mathbf{P}(X = 1) &= 0.184151 & 0.1846 \pm 0.0007 \\ \mathbf{P}(X = 2) &= 0.024513 & 0.02462 \pm 0.00009, \end{aligned}$$

perfectly matching the probabilities extracted from anisotropic sample graphs in the right column (error SEM, c5f1462b). Noting that distance-dependency alone is sufficient to accurately predict edge probabilities in neuron pairs in the anisotropic network model and combined with the observations in Figure 5.7, we conclude that varying degrees of anisotropy do not affect the occurrence of neuron pair motifs.

5.5 TUNING DISTANCE-DEPENDENCY

The discussion in the last section focused on the effect of anisotropy in connectivity on the occurrence of neuron pair motifs. Could distance-dependency itself, as imposed by the specific geometry, be a decisive factor in the distribution of edge counts in neuron pairs? [Song et al. \(2005\)](#), as well as [Perin et al. \(2011\)](#), report an overrepresentation of reciprocal connections independent from distance-dependent connectivity, opposing the observations made in the last section ([Figure 5.7 A](#)). Furthermore, the connectivity profile in the anisotropic graph model, as identified in Section 4.5, follows purely from abstract geometry rather than being motivated by connectivity found in cortical circuits. In an attempt to rectify this and to allow for a more differentiated examination of two neuron connections, in this section we step away from simplistic geometry and “tune” the anisotropic networks to display a distance-dependent connectivity as reported by Perin et al. by adjusting the width $w(x)$ at any point x along the axon’s projection.

For this we introduce anisotropic networks tuned to reflect a given distance-dependent connection profile $C(x)$. We are facing the following problem: Given $C(x) : [0, \sqrt{2}] \rightarrow [0, 1]$, find $w : [0, \sqrt{2}] \rightarrow [0, \infty)$ such that the probability to have a connection from v_1 to v_2 for arbitrary vertices $v_1 \neq v_2$ in an anisotropic graph $G(n, w)$ with distance $d(v_1, v_2) = x$ is $C(x)$. The problem is in general highly complex when nothing can be assumed about $C(x)$. We find an approximate solution to the problem considering the following geometric relation:

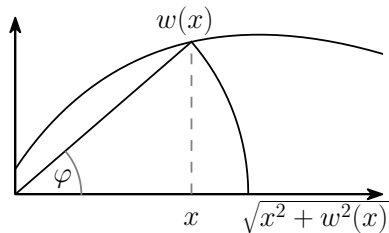


Figure 5.8: Computing connection probability $C(x)$ from non-constant $w(x)$

From [Figure 5.8](#) we have the relation

$$C\left(\sqrt{x^2 + w^2(x)}\right) = \frac{1}{\pi} \arctan \frac{w(x)}{x}. \quad (5.3)$$

In order to solve for $w(x)$ we first consider a linear approximation, expanding

$$C\left(\sqrt{x^2 + w^2(x)}\right) \approx C(x) + \left(\sqrt{x^2 + w^2(x)} - x\right) C'(x).$$

The resulting transcendental equation

$$C(x) + \left(\sqrt{x^2 + w^2(x)} - x \right) C'(x) = \frac{1}{\pi} \arctan \frac{w(x)}{x}$$

is however still too complex in the context of this work. Instead we propose the approximation $\sqrt{x^2 + w^2(x)} \approx x$, which inserting into 5.3 yields

$$C(x) \approx \frac{1}{\pi} \arctan \frac{w(x)}{x}. \quad (5.4)$$

Under the assumption that $C(x) < \frac{1}{2}$ for all x we obtain the identity

$$w(x) = x \tan(\pi C(x)), \quad (5.5)$$

being aware that it only holds as well as approximation 5.4 does.

Here we use relation 5.5 to generate anisotropic networks reflecting the distance-dependent connectivity profile as found by Perin et al. (2011). For this we finally need to adjust the before arbitrarily determined side length of the network's surface. Perin et al. mapped connectivity in layer 5 of the rat's somatosensory cortex up to a distance of 300 µm. Using this reported distance connectivity to generate anisotropic networks via 5.5, the chosen side length s determines the networks overall connectivity (Figure 5.9 A). We determine $s = 296$ µm to match the overall connection probability of $p = 0.116$ as used before and reported by Song et al. (Figure 5.9 B). The obtained value for s is consistent with the slice thickness of 300 µm used in Perin et al.'s experiment.

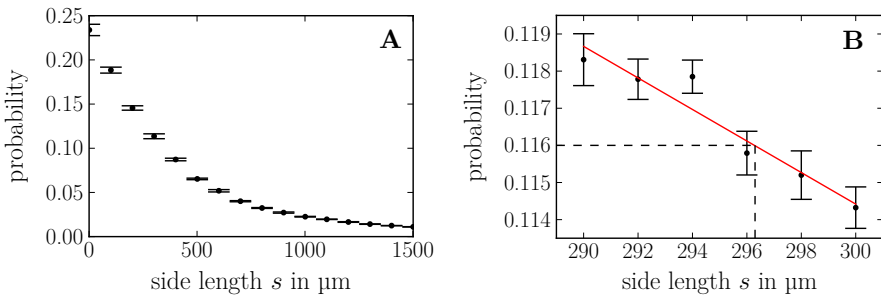


Figure 5.9: Network side length adjusted to match overall connection probability Side length of the network's surface determines the overall connection probability in the network when axon width function $w(x)$ is fixed. **A)** Connection probability declines with rising side length **B)** Determining side length as $s = 296$ µm to match $p = 0.116$ as reported by Song et al. (2005). (6154302f, ef0e785d)

Having determined the network's side length s , we're extending the quiver of generated sample networks for the numerical analysis once more by the “tuned anisotropic graphs”, in which the axon width

$w(x)$ was determined such that the networks reflect Perin's connectivity profile. Analyzing the obtained axon width function we note that $x \gg w(x)$ holds for most x , justifying the approximation

$$\sqrt{x^2 + w^2(x)} \approx x$$

a posteriori (Figure 5.10). From the 25 generated networks overall connection probability is extracted as $p = 0.1160 \pm 0.0006$ (SEM), as expected from the choice of s (f11dca65).

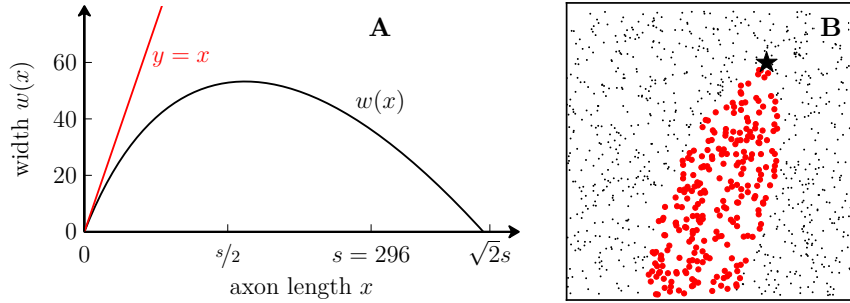


Figure 5.10: Anisotropic network model with tuned axon width $w(x)$ **A)** Resulting axon width function $w(x)$ from tuning to distance-dependent connection profile as reported by Perin et al. (2011), see also Figure 5.11. Note that $x \gg w(x)$ for most x , supporting approximation 5.4. **B)** Showing for a single neuron (star) connected (red) and unconnected (gray) neurons in the tuned anisotropic network, revealing the characteristic axon shape. (d45c02e4, 8f0d65e4)

revisiting two
neuron
connections

Overall distance-dependent connection probabilities in the tuned anisotropic graphs clearly match the profile of Perin et al. (Figure 5.11 A), presenting strongest the argument in support of the chosen approximation. Analyzing two neuron connections in the tuned networks, we affirm the findings of the last section. In their experiment, Perin et al. were able to show an overrepresentation of reciprocal connections at any inter-neuron distance (Figure 5.11 B-C). Rather than matching these profiles, we find that occurrences of one- and bidirectionally connected pairs in the anisotropic graphs align with probabilities obtained from the distance-dependent overall connection probability $p(x)$ under the assumption of independence (cf. Equation 5.5),

$$\begin{aligned} \mathbf{P}_{X=1}(x) &= 2p(x)(1-p(x)) && \text{single connection,} \\ \mathbf{P}_{X=2}(x) &= p(x)^2 && \text{reciprocal connection.} \end{aligned}$$

Thus, in comparison with Perin et al.'s findings, we find that anisotropy in connectivity cannot account for the overrepresentation in reciprocal connections. While results in Section 5.4 still indicated such an overrepresentation due to distance-dependency, examining the occurrence of two neuron connections at any inter-neuron distance in anisotropic

networks tuned to a distance-dependent connection profile matching experimental findings from cortical circuits imply complete unrelatedness of anisotropy and two neuron connection distributions.

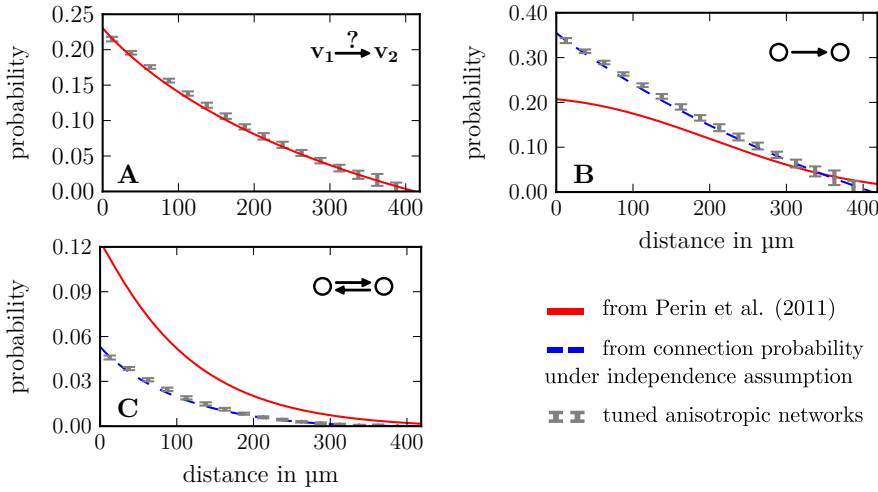


Figure 5.11: Distance-independent overrepresentation of reciprocal connections Comparison of occurrences of one- and bidirectionally connected neuron pairs in the tuned anisotropic networks (gray) with profiles found by Perin et al. (red), shows that overrepresentation of bidirectional pairs is distance-independent and not connected to anisotropy. **A)** Overall connection probability in the tuned anisotropic networks was successfully adjusted to reflect connection probability found by Perin et al. **B)-C)** Showing in blue the probabilities to obtain a neuron pair motif (single edge in B, two edges in C) calculated under independence assumption from the overall probability from A), we find that counts in the tuned anisotropic networks (gray) match the independence assumption and do *not* show the overrepresentation present in Perin et al.'s experiment. (875505b0)

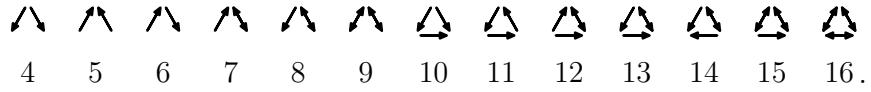
5.6 MOTIFS

In this chapter we analyze the strucarl. The term motif refers to... . Studies of Song et al. (2005) and Perin et al. (2011) show stuff. Pernice2011, Sporns , Zhao2011.

Three-neuron patterns

Here we investigate the occurrence of three-neuron patterns in anisotropic networks. Song et al. (2005) reported a characteristic, highly non-random motif distribution of pyramidal cells in the rat's visual cortex (layer 5), a result later confirmed by Perin et al. (2011) in their experiment in the rat's somatosensory cortex (layer 5). Repeating the experiment *in silico* for the different networks subject to this study, we find similar, characteristic motif distributions strongly influenced by the anisotropy in connectivity.

There are 13^2 three-neuron motifs that represent non-isomorphic, connected simple directed graphs. In reference to Song et al.'s result, the patterns are labeled 4 to 16,



Let X be a random variable that maps three random vertices $v_1 \neq v_2 \neq v_3$ in a graph G to the $n \in \{4, 5, \dots, 16\}$ labeling the isomorphism class of their spanned subgraph in G as above if the subgraph is connected, and let X map to $n = 0$ otherwise. A first idea of how to compute the distribution of X is by inferring the probabilities of motif occurrence from the two-neuron connection probabilities from Section 5.4. In anisotropic networks we found that the probabilities of occurrence are

$$\begin{aligned} p_u &= 0.791336 && \text{for unconnected pairs,} \\ p_s &= 0.184151 && \text{for single connections and} \\ p_r &= 0.024513 && \text{for reciprocal connections.} \end{aligned}$$

From these we may, for example, calculate the probability of occurrence for motif 8,

$$\mathbf{P}(X = 8) = 6 p_u p_s p_r,$$

where the factor 6 is determined by the number of different *labeled* graphs belonging to the isomorphism class. The distribution of X for the remaining motifs is given by

$$\begin{aligned} \mathbf{P}(X = 4) &= 3p_s^2 p_u & \mathbf{P}(X = 9) &= 3p_r^2 p_u & \mathbf{P}(X = 13) &= 6p_s^2 p_r \\ \mathbf{P}(X = 5) &= 3p_s^2 p_u & \mathbf{P}(X = 10) &= 6p_s^3 & \mathbf{P}(X = 14) &= 3p_s^2 p_r \\ \mathbf{P}(X = 6) &= 6p_s^2 p_u & \mathbf{P}(X = 11) &= 2p_s^3 & \mathbf{P}(X = 15) &= 6p_s p_r^2 \\ \mathbf{P}(X = 7) &= 6p_s p_u p_r & \mathbf{P}(X = 12) &= 3p_s^2 p_r & \mathbf{P}(X = 16) &= p_r^3. \end{aligned}$$

² There are 16 simple directed with 3 nodes. Three of those graphs are unconnected (cf. Davis 1953, N. J. A. Sloane. The On-Line Encyclopedia of Integer Sequences, <http://oeis.org>. Sequence A000273).

Does this distribution accurately reflect the occurrences of three-neuron motifs in anisotropic or even distance-dependent networks? Here we take the distribution determined from the two-neuron probabilities as a reference to analyze occurrences of three-neuron motifs in our sets of sample graphs. Counting the occurrences of patterns in we find that there are significant over- and underrepresentations in anisotropic as well as distance-dependent networks, relative to our expectation (Figure 5.12). We find, for example, that in anisotropic graphs pattern 12 occurs almost 5 times as often as we would have expected from the two-neuron probabilities, whereas the counts for pattern 11 only make up less than 30% of the occurrences expected.

distribution from neuron-pairs as reference

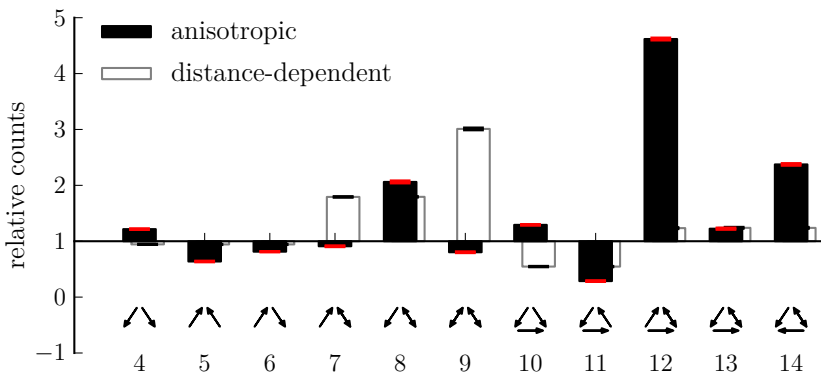


Figure 5.12: Relative occurrence of three-neuron patterns Extracting the counts of three-node motifs in anisotropic (filled bars) and distance-dependent networks (unfilled bars), the quotient of the obtained count with the number of occurrences expected from the two-neuron connection probabilities in the networks (cf. Section 5.4) shows the over- and underrepresentation of specific motifs in the network (red and black errorbars are SEM). In anisotropic networks pattern 12, for example, appears around five times more often than we would expect from the occurrence two-neuron connections. The relative counts for anisotropic networks resemble the findings of Song et al. (2005) and differ significantly from the counts in distance-dependent networks, implying that anisotropy has a strong influence on the relative occurrence of three-neuron patterns. (4839ce41)

*anisotropy
strongly affects
3-motif occurrence*

Comparing the relative counts for motifs in anisotropic graphs with those in comparable distance-dependent networks, we identify a strong influence of anisotropy in connectivity on three-neuron motif occurrence (Figure 5.12). In their experiments, Song et al. and Perin et al. find an overrepresentation of motifs 4, 10, 12 and 14. In anisotropic networks increased counts of motifs 4, 8, 10, 12, 13 and 14 were recorded. However, motifs 8 and 13 are overrepresented in distance-dependent networks as well, leaving the reported motifs 4, 10, 12 and 14 as motifs that are overrepresented due to anisotropy. To analyze this effect

closer, we also compare three-neuron counts before and after rewiring in anisotropic networks (Figure 5.13).

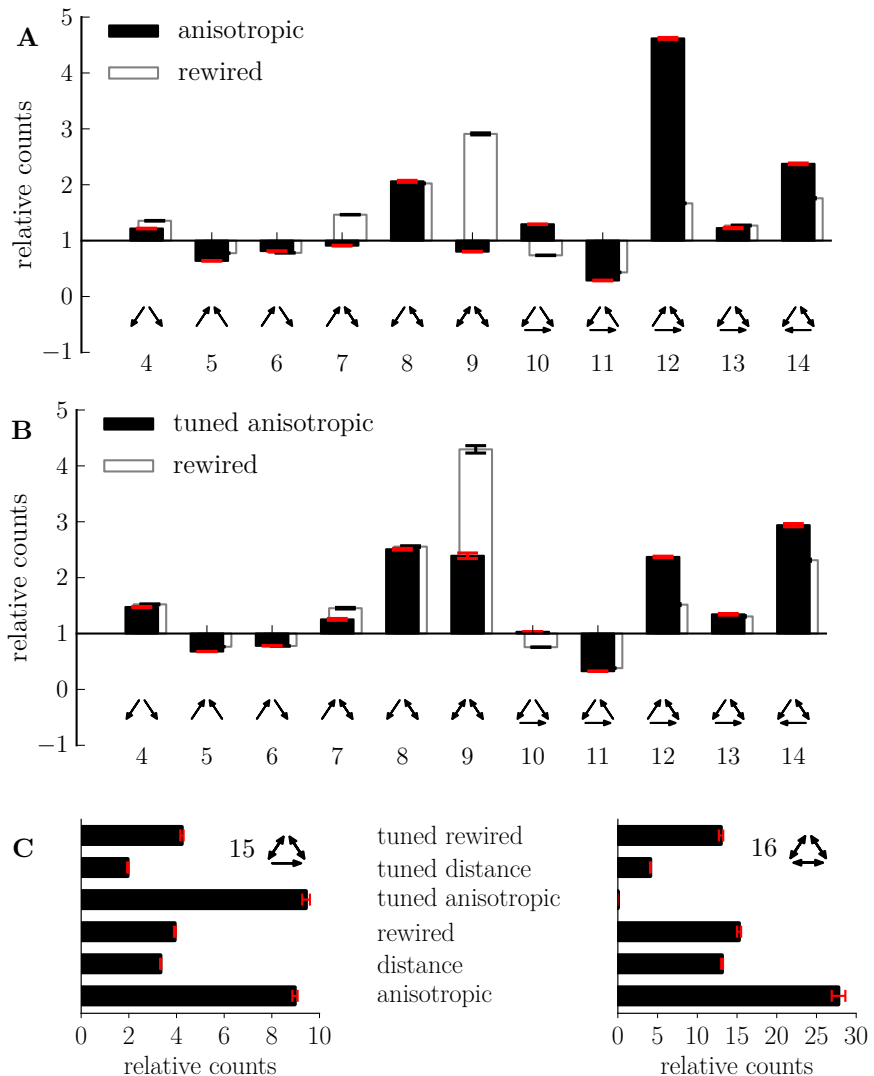


Figure 5.13: Three-neuron motif occurrence in different network types **A)** Comparing counts in anisotropic sample graphs with their rewired counterparts. **B)** Three-neuron motifs occurrence in tuned anisotropic networks (cf. Section 5.5) with their rewired counterparts. For this two-neuron connection probabilities were extracted as in Section 5.4 and motif probabilities were calculated analogously to anisotropic networks. **C)** Relative counts for the high edge count motifs 15 and 16 for different network types, errorbars SEM. (4839ce41)

Considering motif occurrences in anisotropic as well as tuned anisotropic networks, we once again confirm the overrepresentation of motifs 4, 10, 12 and 14. However, increased counts of pattern 4 are observed in the rewired networks as well, leading to the conclusion that increased occur-

rence in this motif is only implicitly affected by anisotropy. Motifs 10, 12 and 14 however show significant overrepresentation even over their rewired counterparts in anisotropic as well as in tuned anisotropic networks.

The overall motif distribution shows itself stable under changes in the distance-dependency with the notable exception of motif 9, that shows underrepresentation only in anisotropic but not in tuned anisotropic or any distance-dependent network type. Analyzing the occurrences of motifs 15 and 16 with a high edge counts ([Figure 5.13 C](#)) we find that anisotropy has strong influence on both motifs, with motif 15 being significantly overrepresented in anisotropic networks. Motif 16 shows a highly increased occurrence in anisotropic networks, however tuning causes the loss of this feature in the network connectivity.

Summarizing the above observations, we find that anisotropy in connectivity induces increased occurrence of motifs 10, 12, 14 and 15 in the network, reflecting experimental results in the rat's cortex. While over- and underrepresentation observed in local cortical circuits can be indirectly linked to anisotropy for some motifs (4, 9) it does not accurately reflect observed counts for other motifs (8) and shows instability under manipulation of distance-dependency in some patterns (9, 16).

results summary

Part I

APPENDIX

A

APPENDIX

A.1 MATHEMATICA

```

In[1]:= f[d_] = Piecewise[{{1 / (s * (d)^(1/2)) - 1 / (s^2), 0 < d < s^2}, {0, d > s^2}}]

Out[1]= 
$$\begin{cases} -\frac{1}{s^2} + \frac{1}{\sqrt{d} s} & 0 < d < s^2 \\ 0 & \text{True} \end{cases}$$


In[2]:= g[x_] := Convolve[f[d], f[d], d, x, Assumptions -> {d ∈ Reals, x ∈ Reals}]
Simplify[g[x], {s > 0, x ∈ Reals}]

Out[3]= 
$$\begin{cases} \frac{\pi s^2 - 4 s \sqrt{x} + x}{s^4} & x > 0 \& s^2 \geq x \\ -\frac{2 s^2 + x + \frac{4 x^3}{\sqrt{-s^2+x}} - \frac{4 x}{\sqrt{-s^2+x}} - 2 s^2 \operatorname{ArcTan}\left[\frac{s}{\sqrt{-s^2+x}}\right] + i s^2 \operatorname{Log}\left[s - i \sqrt{-s^2+x}\right] - i s^2 \operatorname{Log}\left[s + i \sqrt{-s^2+x}\right]}{s^4} & s^2 < x \& 2 s^2 > x \\ 0 & \text{True} \end{cases}$$


In[4]:= h[x_] := g[x^2] * 2 * x

In[5]:= Simplify[h[x], {s > 0, x ∈ Reals, x > 0}]

Out[5]= 
$$2 x \begin{cases} \frac{\pi s^2 - 4 s x + x^2}{s^4} & s \geq x \\ -\frac{2 s^2 + x^2 + \frac{4 x^3}{\sqrt{-s^2+x^2}} - \frac{4 x^2}{\sqrt{-s^2+x^2}} - 2 s^2 \operatorname{ArcTan}\left[\frac{s}{\sqrt{-s^2+x^2}}\right] + 2 s^2 \operatorname{ArcTan}\left[\frac{\sqrt{-s^2+x^2}}{s}\right]}{s^4} & s < x \& \sqrt{2} s > x \\ 0 & \text{True} \end{cases}$$


In[6]:= (*For s == 1, h becomes*)

In[7]:= Simplify[h[x], {s == 1, x ∈ Reals, x > 0}]

Out[7]= 
$$2 x \begin{cases} \pi + (-4 + x) x & x \leq 1 \\ -2 - x^2 + 4 \sqrt{-1 + x^2} - 2 \operatorname{ArcCot}\left[\frac{1}{\sqrt{-1+x^2}}\right] + 2 \operatorname{ArcTan}\left[\frac{1}{\sqrt{-1+x^2}}\right] & 1 < x < \sqrt{2} \\ 0 & \text{True} \end{cases}$$


In[8]:= (*Expected Value*)
s := 1.
Integrate[x * h[x], {x, 0, Sqrt[2]}]

Out[9]= 0.521405

```

Mathematica A.1: Computation of probability density function for distance between two random points in square of side length s as supplement to proof of Theorem 3.14. Note that form of final result Out[7] differs from solution given in 3.14. While proof of equivalence could not be achieved analytically, expressions given are numerically equivalent, see Mathematica A.2.

```

In[1]:= f[d_] = Piecewise[{{1 / (s * (d)^(1/2)) - 1 / (s^2), 0 < d < s^2}, {0, d > s^2}}]

Out[1]= 
$$\begin{cases} -\frac{1}{s^2} + \frac{1}{\sqrt{d}} & 0 < d < s^2 \\ 0 & \text{True} \end{cases}$$


In[2]:= g[x_] := Convolve[f[d], f[d], d, x, Assumptions -> {d ∈ Reals, x ∈ Reals}]
Simplify[g[x], {s > 0, x ∈ Reals}]

Out[3]= 
$$\begin{cases} \frac{\pi s^2 - 4 s \sqrt{x} + x}{s^4} & x > 0 \& s^2 \geq x \\ -\frac{2 s^2 + x + \frac{4 s^3}{\sqrt{-s^2+x}} - \frac{4 s x}{\sqrt{-s^2+x}} - 2 s^2 \operatorname{ArcTan}\left[\frac{s}{\sqrt{-s^2+x}}\right] + i s^2 \operatorname{Log}[s-i \sqrt{-s^2+x}] - i s^2 \operatorname{Log}[s+i \sqrt{-s^2+x}]}{s^4} & s^2 < x \& 2 s^2 > x \\ 0 & \text{True} \end{cases}$$


In[4]:= h[x_] := g[x^2] * 2 * x

In[5]:= Simplify[h[x], {s > 0, x ∈ Reals, x > 0}]

Out[5]= 
$$2 x \begin{cases} \frac{\pi s^2 - 4 s x + x^2}{s^4} & s \geq x \\ -\frac{2 s^2 + x^2 + \frac{4 s^3}{\sqrt{-s^2+x^2}} - \frac{4 s x^2}{\sqrt{-s^2+x^2}} - 2 s^2 \operatorname{ArcTan}\left[\frac{s}{\sqrt{-s^2+x^2}}\right] + 2 s^2 \operatorname{ArcTan}\left[\frac{\sqrt{-s^2+x^2}}{s}\right]}{s^4} & s < x \& \sqrt{2} < x \\ 0 & \text{True} \end{cases}$$


In[6]:= (*For s == 1, h becomes*)

In[7]:= Simplify[h[x], {s == 1, x ∈ Reals, x > 0}]

Out[7]= 
$$2 x \begin{cases} \pi + (-4 + x) x & x \leq 1 \\ -2 - x^2 + 4 \sqrt{-1 + x^2} - 2 \operatorname{ArcCot}\left[\frac{1}{\sqrt{-1+x^2}}\right] + 2 \operatorname{ArcTan}\left[\frac{1}{\sqrt{-1+x^2}}\right] & 1 < x < \sqrt{2} \\ 0 & \text{True} \end{cases}$$


In[8]:= (*Expected Value*)
s := 1.
Integrate[x * h[x], {x, 0, Sqrt[2]}]

Out[9]= 0.521405

```

Mathematica A.2: Computation of probability density function for distance between two random points in square of side length s as supplement to proof of Theorem 3.14. Note that form of final result Out[7] differs from solut

A.2 SUPPLEMENTARY FIGURES

Chapter 4

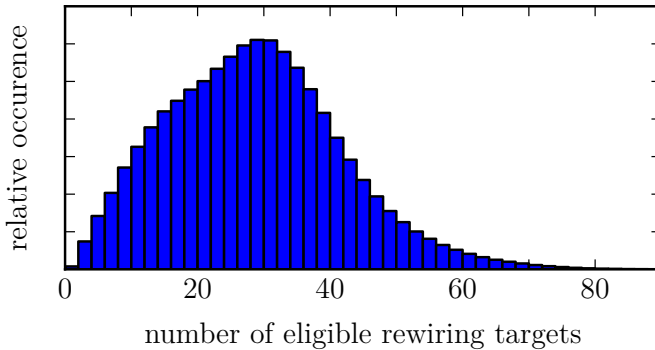
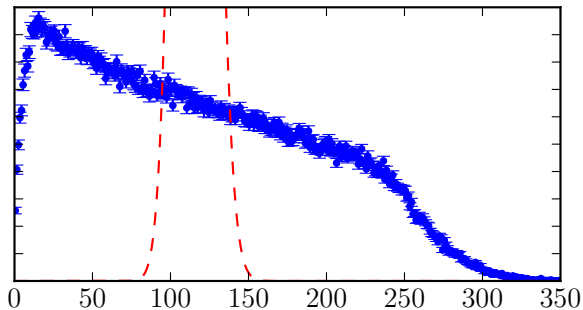
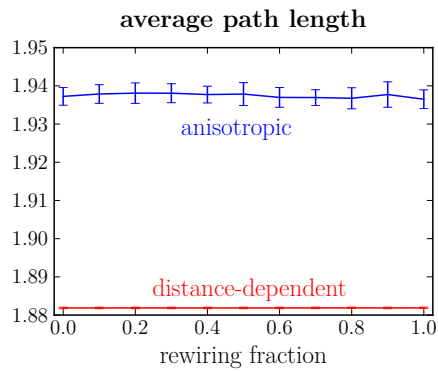
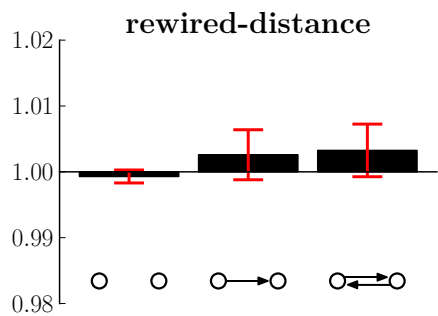


Figure A.1: (4afc2727)

Chapter 5

**Figure A.2:** (c7ee86d7)**Figure A.3:** Average path length for anisotropic and distance-dependent networks, $N = 1000$. (064f9b10)**Figure A.4:** Probabilities for connections in neuron pairs are identical in distance-dependent and rewired anisotropic networks. (c5f1462b)

BIBLIOGRAPHY

- Achard, Sophie and Ed Bullmore (2007). Efficiency and Cost of Economical Brain Functional Networks. *PLoS Comput Biol* 3.2, e17. DOI: 10.1371/journal.pcbi.0030017.
- Bang-Jensen, Jørgen and Gregory Z. Gutin (2008). *Digraphs: Theory, Algorithms and Applications*. 2nd ed. London: Springer. DOI: 10.1007/978-1-84800-998-1.
- Bassett, Danielle Smith and Ed Bullmore (2006). Small-World Brain Networks. *The Neuroscientist* 12.6, pp. 512–523. DOI: 10.1177/1073858406293182.
- Bollobás, Béla (2001). *Random graphs*. 2nd ed. Cambridge University Press.
- Braitenberg, Valentino and A Schüz (1998). *Cortex: Statistics and Geometry of Neuronal Connectivity*. 2nd ed. Berlin; New York: Springer.
- Brette, Romain and Alain Destexhe (2012). *Handbook of neural activity measurement*. Cambridge: Cambridge University Press.
- Davis, Robert L. (1953). The Number of Structures of Finite Relations. *Proceedings of the American Mathematical Society* 4.3, pp. 486–495.
- Debanne, Dominique (2004). Information processing in the axon. *Nature Reviews Neuroscience* 5.4, pp. 304–316.
- Diestel, Reinhard (2000). *Graph Theory*. 2nd ed. Vol. 173. Graduate Texts in Mathematics. Springer-Verlag, New York.
- Erdős, P. and A. Rényi (1959). On random graphs, I. *Publicationes Mathematicae (Debrecen)* 6, pp. 290–297.
- Feldman, ML (1984). Morphology of the neocortical pyramidal neuron. *Cerebral cortex, Vol 1, Cellular components of the cerebral cortex*. Ed. by Alan Peters and Edward G Jones. New York: Plenum Press, pp. 123–200.
- Gilbert, E. N. (1959). Random Graphs. *The Annals of Mathematical Statistics* 30.4, pp. 1141–1144. DOI: 10.1214/aoms/1177706098.
- Gilbert, E.N. (1961). Random Plane Networks. *Journal of the Society for Industrial and Applied Mathematics* 9.4, pp. 533–543. DOI: 10.1137/0109045.
- Holmgren, Carl, Tibor Harkany, Björn Svennensfors, and Yuri Zilberman (2003). Pyramidal cell communication within local networks in

- layer 2/3 of rat neocortex. *The Journal of Physiology* 551.1, pp. 139–153. DOI: 10.1113/jphysiol.2003.044784.
- Ishizuka, Norio, Janet Weber, and David G Amaral (1990). Organization of intrahippocampal projections originating from CA3 pyramidal cells in the rat. *Journal of Comparative Neurology* 295.4, pp. 580–623.
- Janson, S., T. Łuczak, and A. Rucinski (2000). *Random Graphs*. Wiley Series in Discrete Mathematics and Optimization. Wiley.
- Klinshov, Vladimir V., Jun-nosuke Teramae, Vladimir I. Nekorkin, and Tomoki Fukai (2014). Dense Neuron Clustering Explains Connectivity Statistics in Cortical Microcircuits. *PLoS ONE* 9.4, e94292. DOI: 10.1371/journal.pone.0094292.
- Ko, Ho, Sonja B. Hofer, Bruno Pichler, Katherine A. Buchanan, P. Jesper Sjöström, and Thomas D. Mrsic-Flogel (2011). Functional specificity of local synaptic connections in neocortical networks. *Nature* 473.7345, pp. 87–91. DOI: 10.1038/nature09880.
- Łuczak, Tomasz (1990). On the equivalence of two basic models of random graph. *Proceedings of Random graphs*. Vol. 87, pp. 151–157.
- Mardia, Kanti V. and Peter E. Jupp (2000). *Directional Statistics*. 2nd ed. John Wiley & Sons Ltd.
- Markram, H. (1997). A network of tufted layer 5 pyramidal neurons. *Cerebral cortex (New York, N.Y. : 1991)* 7.6, pp. 523–533. DOI: 10.1093/cercor/7.6.523.
- Moltchanov, D. (2012). Distance distributions in random networks. *Ad Hoc Networks* 10.6, pp. 1146–1166. DOI: 10.1016/j.adhoc.2012.02.005.
- nLab (2014). *Graph*. URL: <http://ncatlab.org/nlab/revision/graph/56>.
- Penrose, Mathew (2003). *Random Geometric Graphs (Oxford Studies in Probability)*. Oxford University Press, USA.
- Perin, Rodrigo, Thomas K. Berger, and Henry Markram (2011). A synaptic organizing principle for cortical neuronal groups. *Proceedings of the National Academy of Sciences* 108.13, pp. 5419–5424. DOI: 10.1073/pnas.1016051108.
- Pernice, Volker, Benjamin Staude, Stefano Cardanobile, and Stefan Rotter (2011). How Structure Determines Correlations in Neuronal Networks. *PLoS Comput Biol* 7.5, e1002059. DOI: 10.1371/journal.pcbi.1002059.
- Petersen, Carl C. H., Amiram Grinvald, and Bert Sakmann (2003). Spatiotemporal Dynamics of Sensory Responses in Layer 2/3 of Rat Barrel Cortex Measured In Vivo by Voltage-Sensitive Dye Imaging

- Combined with Whole-Cell Voltage Recordings and Neuron Reconstructions. *The Journal of Neuroscience* 23.4, pp. 1298–1309.
- Philip, J. (2007). The probability distribution of the distance between two random points in a box. TRITA MAT 07 MA 10.
- Ramaswamy, Srikanth, Sean L Hill, James G King, Felix Schürmann, Yun Wang, and Henry Markram (2012). Intrinsic morphological diversity of thick-tufted layer 5 pyramidal neurons ensures robust and invariant properties of in silico synaptic connections. *The Journal of physiology* 590.4, pp. 737–752.
- Ramon, Y and S Cajal (1911). Histologie du systeme nerveux de l'homme et des vertebres. *Maloine, Paris* 2, pp. 153–173.
- Romand, Sandrine, Yun Wang, Maria Toledo-Rodriguez, and Henry Markram (2011). Morphological development of thick-tufted layer V pyramidal cells in the rat somatosensory cortex. *Frontiers in Neuroanatomy* 5.5. DOI: 10.3389/fnana.2011.00005.
- Ropireddy, Deepak, Ruggero Scorcioni, Bonnie Lasher, Gyorgy Buzsáki, and Giorgio A. Ascoli (2011). Axonal morphometry of hippocampal pyramidal neurons semi-automatically reconstructed after in vivo labeling in different CA3 locations. *Brain Structure and Function* 216.1, pp. 1–15. DOI: 10.1007/s00429-010-0291-8.
- Roxin, Alex (2011). The Role of Degree Distribution in Shaping the Dynamics in Networks of Sparsely Connected Spiking Neurons. *Frontiers in Computational Neuroscience* 5. DOI: 10.3389/fncom.2011.00008.
- Simpson, Thomas (1755). A letter to the Right Honourable George, Earl of Macclesfield, President of the Royal Society, on the advantage of taking the mean of a number of observations in practical astronomy. *Phil. Trans. R. Soc. Lond* 49, pp. 82–93.
- Song, Sen, Per Jesper Sjöström, Markus Reigl, Sacha Nelson, and Dmitri B Chklovskii (2005). Highly Nonrandom Features of Synaptic Connectivity in Local Cortical Circuits. *PLoS Biol* 3.3, pp. 507–519. DOI: 10.1371/journal.pbio.0030068.
- Sporns, Olaf (2007). Brain connectivity. *Scholarpedia* 2.10, p. 4695. DOI: 10.4249/scholarpedia.4695.
- Sporns, Olaf and Rolf Kötter (2004). Motifs in Brain Networks. *PLoS Biol* 2.11, e369. DOI: 10.1371/journal.pbio.0020369.
- Sporns, Olaf and Jonathan D. Zwi (2004). The small world of the cerebral cortex. *Neuroinformatics* 2.2, pp. 145–162. DOI: 10.1385/NI:2:2:145.
- Stepanyants, Armen and Dmitri B. Chklovskii (2005). Neurogeometry and potential synaptic connectivity. *Trends in Neurosciences* 28.7, pp. 387 –394. DOI: 10.1016/j.tins.2005.05.006.

- Stepanyants, Armen, Patrick R. Hof, and Dmitri B. Chklovskii (2002). Geometry and Structural Plasticity of Synaptic Connectivity. *Neuron* 34.2, pp. 275 –288. DOI: 10.1016/S0896-6273(02)00652-9.
- Watts, Duncan J. and Steven H. Strogatz (1998). Collective dynamics of 'small-world' networks. *Nature* 393.6684, pp. 440–442. DOI: 10.1038/30918.
- Weckstrom, Matti (2010). Intracellular recording. *Scholarpedia* 5.8, p. 2224. DOI: 10.4249/scholarpedia.2224.
- Zhao, Liqiong, Bryce Beverlin, Theoden Netoff, and Duane Q. Nykamp (2011). Synchronization from Second Order Network Connectivity Statistics. *Frontiers in Computational Neuroscience* 5. DOI: 10.3389/fncom.2011.00028.

INDEX

anisotropic geometric
graph, 24
random graph model, 24
apical dendrite, 20

basal dendrite, 20
binomial random graph, 11

directed graph, 5
distance-dependent
 connection probability, 12
 connection profile, 12
 random graph model, 12

geometric graph, 11
Gilbert random graph model, 10

in-degree, 7

loop graph, 5

multigraph, 5

neuro geometry, 18

out-degree, 7

potential synapse, 18
preferred direction, 33
pseudograph, 5

random graph, 9

simple graph, 5

tuned anisotropic networks, 47

weighted graph, 6

Symbol	Description
$\mathcal{B}_{n,p}$	Binomial distribution with n trials and a success rate of p
SEM	standard error of the mean